

Finding suitable material for the retaining sleeves in the tidal generators.

Avinash Yadav

Master of Science Thesis

Finding suitable material for the retaining sleeves in the tidal generators.

by

Avinash Yadav

to obtain the degree of Master of Science
at the Delft University of Technology,
to be defended publicly on Tuesday August 24, 2017 at 10:00 AM.

Student number : 4515196

Thesis committee : Dr. ir. Henk Polinder, TU Delft, supervisor
Dr. Jianning Dong, TU Delft
Dr. Hayo Hendrikse, TU Delft

This thesis is confidential and cannot be made public until August 24, 2017.

An electronic version of this thesis is available at <http://repository.tudelft.nl/>.

Abstract

Tidal energy is one of form through which renewable energy can be extracted from oceans which covers more than 70% of the earth surface. Tides are a periodic function and can be predicted for a long period this makes tidal energy more favorable than other ocean energy. To prevent the sealing problems associated with the tidal generators the stator-rotor gap is flooded with seawater. Insulating sleeves are used to overcome issues of corrosion of the permanent magnets and the electrical insulation which arises due to the flooding of the stator-rotor gap. The aim of the thesis is to suggest a suitable material that can be used for the insulating sleeve based on the eddy current loss and temperature of the generator. Magnetohydrodynamics is other phenomena that will arise due to flooding of the stator-rotor gap of the tidal generator. Losses associated with Magnetohydrodynamics are also evaluated.

The geometrical parameters of the generator are calculated based on the required power rating and the average velocity of the tides. The eddy current losses in the insulating sleeves are evaluated analytically by calculating the magnetic flux density in the insulating sleeves. A thermal model of the machine is developed to investigate the temperature distribution inside the generator due to different materials of the insulating sleeves to derive at the suggestion for the material to be used.

It is observed that the Magnetohydrodynamics losses are not significant as compared to the other losses. It is also found that the steel is a suitable material which can be used on the rotor while for stator non-metallic material will be most suitable.

Preface

Firstly, I would like to express my gratitude to my supervisor Henk Polinder, for providing me the opportunity to work in this research and for his guidance during the monthly meetings without which I would never have been able to find my way.

I would am grateful to Jianning Dong and Udai Shipurkar for many valuable discussions involving thesis. Their knowledge of the electrical machines helped me understand many phenomena.

I would like to thank Faisal Wani who was my daily supervisor for all the time and effort he devoted to me during the thesis. Your suggestions and corrections in my draft thesis help me write my thesis in a better way.

And finally, I want to thank my family and friends for their continued support.

Delft, University of Technology
September 4, 2017

Avinash Yadav

Table of Contents

Preface	iii
1 Introduction	1
1-1 Background	1
1-2 Motivation	3
1-3 Literature Review	3
1-4 Problem Statement and Research Objective	4
1-5 Thesis Structure	4
2 Analytical Design of Machine	7
2-1 Introduction	7
2-2 Choices	7
2-3 Analytical Model for Generator Design	9
2-3-1 Material Volume and Weight	12
2-4 Losses	13
2-4-1 Copper Losses	13
2-4-2 Core Losses	13
2-4-3 Losses in the Permanent Magnets	14
2-5 Results	14
3 Analytical Model for Loss Calculation	17
3-1 Introduction	17
3-2 Mathematical Model	17
3-3 Boundary Conditions	19
3-4 Skin Depth	19
3-5 Magnetic Field due to Magnets	20
3-6 Current Sheet Distribution	21

3-7	Magnetic Flux due to Armature Winding	21
3-8	Effect of Stator Slotting	24
3-9	Slotted Machine Results	25
3-10	Retaining Sleeve Material	25
3-11	Eddy Current Induced in the Retaining Sleeve	27
3-12	Results	28
3-13	Conclusion	29
4	Magnetohydrodynamics	31
4-1	Introduction	31
4-2	Taylor - Couette Flow	31
4-3	The MHD Model	32
4-4	MHD Losses	35
4-5	Conclusion	37
5	Thermal Model	39
5-1	Introduction	39
5-2	Thermal Model	39
5-2-1	Thermal Conduction	39
5-2-2	Thermal Convection	43
5-2-3	Heat Transfer Coefficient	43
5-2-4	Thermal Radiation	44
5-3	Models of Thermally Conductive Parts	44
5-3-1	Thermal Model of Stator and Rotor Yoke	44
5-3-2	Thermal Model of Stator Teeth	45
5-3-3	Thermal Model of Stator Winding	45
5-3-4	Thermal Model of the Retaining Sleeves	46
5-3-5	Thermal Model of Airgap	46
5-3-6	Thermal Model of End Winding	46
5-3-7	Thermal Model of Permanent Magnet	47
5-3-8	Thermal Model of End Cap	48
5-3-9	Thermal Model of The Shaft	48
5-4	Results	48
6	Conclusion and Recommendations	51
A	General solution of Laplace equation	53
B	Star of slot method	55
C	Magnetohydrodynamics	57
D	Thermal Model	59

List of Figures

1-1	World wide tidal energy potential [1]	2
1-2	Outline of this thesis	5
2-1	Horizontal axis tidal generator [3]	8
2-2	Vertical axis tidal generator [2]	8
2-3	Cross section of Rim driven permanent magnet generator [4]	9
2-4	The slot and single layer winding	11
2-5	Magnetic flux density at A-A position due to different pole pair numbers.	16
2-6	FEM result of No load magnetic flux density for integral slot winding machine	16
3-1	Skin depth calculated at different harmonic order	19
3-2	Cross section of slot less internal rotor machine [5]	20
3-3	Radial magnetic flux density due to the PM for slotless machine derived at the center of the stator-rotor gap.	22
3-4	Current Density due single winding	22
3-5	Magnetic flux density due to the armature winding for slotless machine derived at the center of the stator-rotor gap.	24
3-6	Permeance calculation model [6]	24
3-7	Analytical PM field(slotted)vs FEM field	26
3-8	Analytical armature winding field(slotted)vs FEM field	26
3-9	Retaining sleeve configurations	27
3-10	Induced Current density in rotor retaining sleeve at outer radii (B-B position) for Inconel material.	28
4-1	Schematic representation of the Taylor-Couette-Poiseuille configuration with relevant notations [7]	32
4-2	Fluid velocity variation for different values of the magnetic flux density radially	34

4-3	Electromechanical power transmitted vs stator rotor gap in radial direction evaluated by using Equation 4-14	34
4-4	Eddy currents in the stator-rotor gap for different values of the magnetic flux densities radially	35
4-5	Eddy currents in the stator-rotor gap for stationary and rotating seawater . . .	36
4-6	Seawater velocity under no load condition	36
5-1	Basic Thermal Model [8]	40
5-2	Combined thermal network for symmetric component	41
5-3	Percentage of error in thermal resistance at different ratio of r_2/r_1	42
5-4	Thermal Model of stator teeth	45
5-5	Thermal Model of Permanent Magnet region	47
5-6	The node placement for the thermal model	49
B-1	Example of star of slots of machine with $Q = 9, 2p = 8$ [9]	56
C-1	Velocity variation seawater at different rotor velocity	57
C-2	Current Density in seawater at different rotor velocity	58
D-1	Thermal Model of Machine	61

List of Tables

2-1	Geometrical Parameters of the machine	9
2-2	Assumed variables for the machine	14
2-3	Geometric parameters of the Integer slot winding machine	15
2-4	Losses	15
3-1	Machine regions defined for calculating the vector potential from Equation (3-15)	20
3-2	Different materials used as insulation material	26
3-3	Eddy current losses for various rotor retaining sleeve material	28
3-4	Eddy current losses in stator retaining sleeve for various material	29
3-5	Eddy current losses in rotor retaining sleeve for Integral slot winding machine	29
4-1	Reynolds number calculated for different machine dimension	32
4-2	Loss associated With MHD	37
5-1	Thermal conductance of different materials	49
5-2	Temperature in different part of the machine with only rotor retaining sleeve .	49
5-3	Temperature in different part of the machine with copper sleeve and rotor retaining sleeve	50
5-4	Temperature in different part of the machine with stator and rotor retaining sleeve	50
B-1	Harmonic Orders(HO) of a single-layer winding [10]	56
D-1	Thermal resistances and their explanations of the network	59

Chapter 1

Introduction

1-1 Background

As oceans cover more than 70% of the earth's surface, they can offer abundant resources for renewable energy which is much higher than that obtained from any other source[11]. Theoretically, the ocean could produce much more energy than human race could use. Ocean energy is available in different forms as indicated below:

- Wave energy.
- Marine current energy (tidal energy).
- Osmotic energy (energy from salinity gradients).
- Ocean thermal energy.
- Cultivation of marine biomass.

Offshore wind farms and offshore solar plants are other renewable energy that can be extracted from the ocean, but the primary source of energy extraction is not the ocean. Wave energy and tidal energy are the most advanced and are expected to contribute significantly to the supply of energy among the other ocean energy forms [12]. Osmotic energy or Salinity gradient power is the energy generated due to the difference in salt concentration between two fluids, commonly fresh and salt water. Pressure Retarded Osmosis (PRO) and Reversed Electro Dialysis (RED) are the two major technologies for osmotic energy. Ocean thermal energy produces electricity from the natural thermal gradient of the ocean, using the heat stored in warm surface water to create steam to drive a turbine while pumping cold, deep water to the surface to recondense the steam. Ocean thermal energy plants can be either built onshore or on offshore floating platforms.

Tidal phenomena are periodic. The exact nature of the periodic response varies according to the interaction between respective movements of the moon and the sun, the gravitation effects, and other geographical peculiarities. The tidal change typically occurs twice daily, the main periods being

diurnal (24 hours and 50 minutes) and semidiurnal (12 hours, 25 minutes). Tidal waveforms can be predicted for a long period, this predictability of tides makes marine current energy (tidal energy) more attractive than any other renewable energy sources. Connecting tidal energy to the electrical grid is easy due to the predictability of the tides [13]. Electricity can be generated from tidal energy in two ways either by building a tidal barrage across an estuary or a bay, or by harnessing energy from free flowing tidal currents [3]. An economically feasible location for tidal energy should have peak tidal current velocities higher than 2m/s, these can be found only at select locations across the globe, such as in straits between shallows around headlands and in between islands and the mainland as shown in Fig. 1-1 [14]. The total worldwide potential for tidal energy is 0.5TW [1]. Despite the enormous potential for harnessing energy from the tidal waves, it has remained relatively under-exploited. The risk of marine environment such as extreme weather, corrosion and fouling has been a bottleneck for this sector to acquire finances to drive the growth in technology [2].

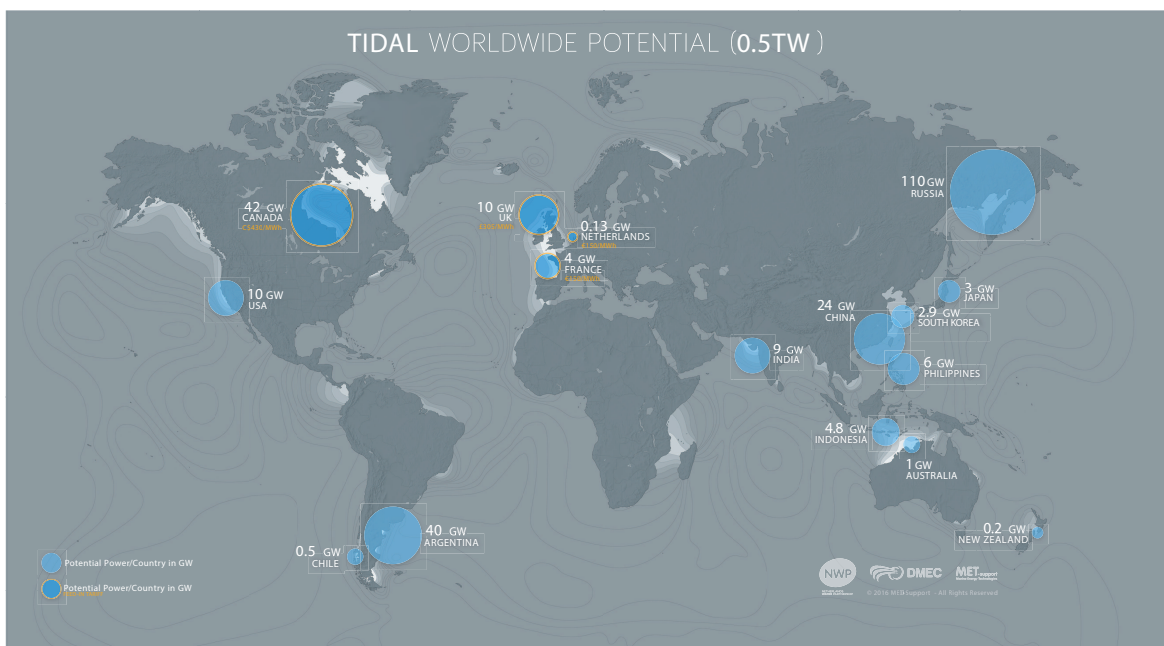


Figure 1-1: World wide tidal energy potential [1]

Tidal generators allow designers to limit visual exposure as well as acoustic disturbances and also to reduce environmental impact [13]. However, immersion of such a system in seawater requires tidal generators to be ultra reliable in the marine environment and to have waterproof technologies [13]. The flooding of generators saves problems associated with the sealing of generators, but it induces many critical challenges, some of which are listed below.

1. Corrosion protection of the NdFeB permanent magnets.
2. Increased fluid drag loss as water fills the stator-rotor gap.
3. Electrical insulation problem.
4. Necessity to modify the bearing design.

The corrosion of NdFeB magnets occurs through intergranular attack derived from the preferential consumption of Nd-rich and Be-rich phases on the grain boundaries which causes the grains of the ferromagnetic phases to loosen thereby leading to the formation of pits [15]. The corrosion resistance of the magnets can be improved by adopting methods such as doping and surface coating either with epoxy resin or Al or Ni. Because of the water absorbing properties of the epoxy, Al/Ni are better options for the corrosion protection of permanent magnets [16]. To protect the magnets from corrosion and windings from insulation failure protective layer of metallic or non-metallic material can be used. In the case of high-speed machines, the protective layer is used to prevent the magnets from cracking due to centrifugal force experienced by the magnets [17]. For high-speed machines, this protective layer is also known as retaining sleeve.

1-2 Motivation

Retaining sleeves are used to protect the active parts of the tidal generators. Eddy currents will be induced in the retaining sleeve due to spatial harmonics if the sleeve is made of metallic material. The induced eddy currents in a low-speed machine are not as significant as that in high-speed machines, but their significance needs to be evaluated. The metallic sleeve may also work as a magnetic shield and will reduce the eddy currents in the magnets and the rotor yoke.

Due to flooding of the tidal generators seawater is present in the stator-rotor gap, as the seawater is electrically conductive magnetohydrodynamics (MHD) phenomena will be seen in the stator-rotor gap. Friction and Joule losses are the major losses observed due to the MHD. The electrical conductivity of the seawater is very low as compared to the metallic retaining sleeve hence the Joule loss due to MHD in stator-rotor gap will be small, but they are part of non-conventional losses and deserve to be quantified.

The thesis is focused on finding a suitable material or combination of material that can be used in the retaining sleeves of the tidal generators considering eddy current loss, corrosion protection, and better thermal conductivity.

1-3 Literature Review

Long life time and low or zero on board maintenance are the essential requirements for wave and tidal generators while corrosion and failure of the sealing equipment are the biggest challenges for the fully submerged machine [18] [19]. The design approach for tidal generators have been proposed in [4], [14], [20], and [13]. In [20], the author has proposed the design for a POD type permanent magnet tidal generator, In [14], the author has proposed the design for a rim driven tidal generator for sail boat application, and in [21], [13] author gives the analysis of axial flux permanent magnets for tidal generators. It is observed in the design approach studied before that eddy current losses in the rotor retaining sleeve are not considered, the rotor retaining sleeve materials are also not taken into account. The importance of eddy evaluation can be observed in [22], [23], [24], [25], [26], [27], [28]. In [27] and [28] authors have developed an analytical model for eddy current calculation in canned induction machine, while in [26] author has studied the eddy current losses in the retaining sleeve considering different materials as well. In [25] and [24] authors have developed models to quantify the eddy current loss in rotor yoke and permanent magnets for a permanent magnet brushless

machine, while [22] and [23] authors show the importance of eddy current losses in the retaining sleeve for high-speed permanent magnet brushless machine. The study also shows the advantage of using a conductive shield in retaining sleeve and its influence on rotor loss. The study conducted in [29] also demonstrates the advantage of using a conductive shield in reducing the eddy losses, It also shows the advantage of using axial segmentation of retaining sleeves in eddy loss reduction. Of all the research reviewed, it is felt that there is a need for study of eddy current losses in low-speed tidal generators and look at which kind of sleeve material will be suitable for tidal generator application.

To determine whether a material is suitable to be used in a machine, its thermal properties should also be studied. Lumped circuit thermal model of the machine is developed in [8] and [30] based on the dimensions of different machine region and thermal properties of the material used. But the machine used is induction machine with air in the stator-rotor gap. The [31] build a detailed thermal of switched reluctance machine, the thermal resistances for the end cap more detailed than that in [8]. The Nusselt numbers used in the [31] are reevaluated and confirmed in [32].

Other phenomena observed in flooded tidal generators is MHD, In [33] showed MHD losses in stator-rotor gap, flooded with seawater, are not of significant value as compared to other losses. But the study performed was for small gap values while the stator-rotor gap for a large diameter machine is between 5mm-10mm. It will be interesting to evaluate the MHD losses for higher gap values under harmonic magnetic flux density.

1-4 Problem Statement and Research Objective

The problem statement is *Finding suitable material for the retaining sleeves in the tidal generators.* The research objectives are as follows:

1. Evaluation of the eddy current losses in the retaining sleeves of different material and the permanent magnet.
2. Evaluate temperature in the tidal generator for the different retaining sleeve materials and find a suitable material for retaining sleeve.
3. Evaluate the significance of Magnetohydrodynamics (MHD) loss in the tidal generators.

1-5 Thesis Structure

To achieve the objectives mentioned above, this thesis is organized as shown in the flow chart given in Fig. 1-2.

In Chapter 2, choices are made between different configurations and machine parameters, such as the POD type or the RIM type configurations of the machine, whether the machines are axial or radial flux. The initial design of the machine is based on these selections. Chapter 3 focuses on the analytical modeling for the magnetic flux density in the stator-rotor gap attributed to the permanent magnets and the armature fields, and the machine losses are calculated based on that. Chapter 4 explores Magnetohydrodynamics (MHD) loss in the stator-rotor gap while considering harmonics in the magnetic flux density. Chapter 5 examines the thermal circuit model of the machine to understand the temperature distribution inside the machine emanating from the use of different types of retaining

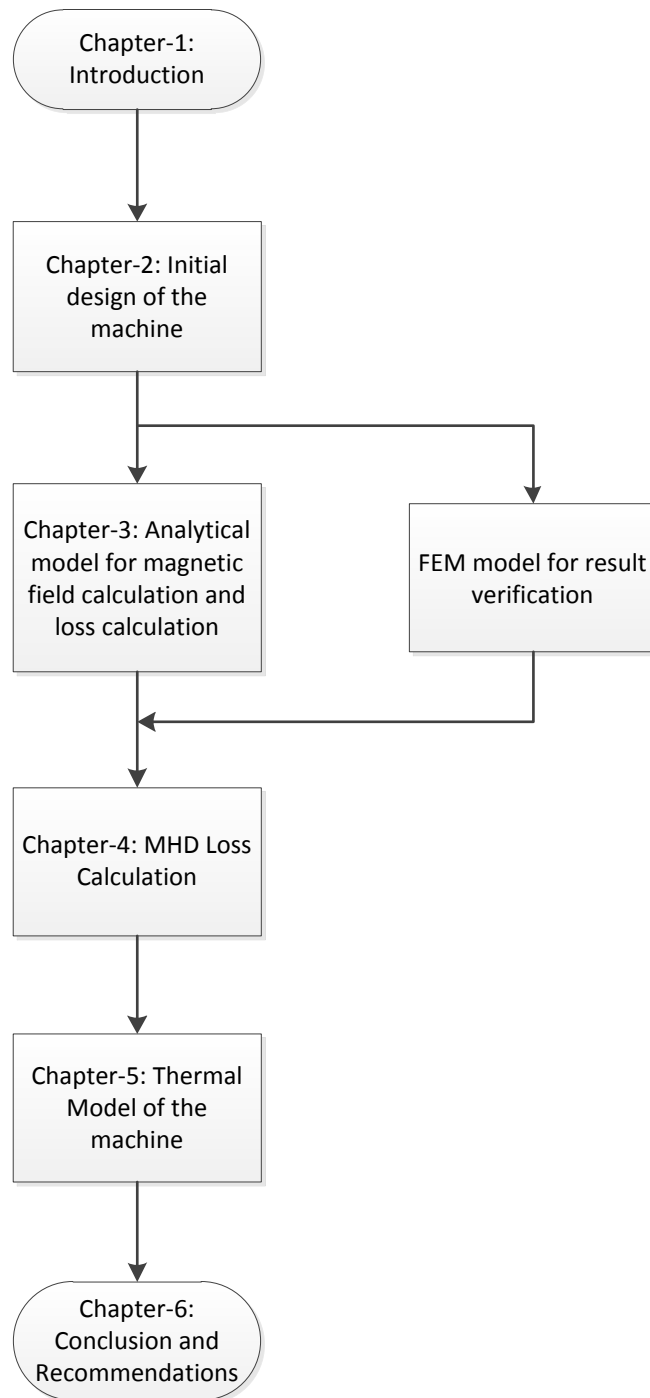


Figure 1-2: Outline of this thesis

sleeve material. In Chapter 6 the report concludes by providing a brief review of all the conclusions drawn in the previous chapters to address the research objectives and further recommendations for future work.

Chapter 2

Analytical Design of Machine

2-1 Introduction

The objective of the chapter is to calculate the geometrical parameters of the tidal generators. The chapter first discusses the different choices based on which type of the machine is selected. Secondly, it shows the approach adopted for calculation of the machine parameters. Later on, it will discuss the assumptions and results.

2-2 Choices

HATT or VATT

Over the past decade several designs of the tidal generators have been proposed, but due to various reasons not all of them have been realized. One of the most common and prominently visible types are the horizontal axis tidal turbine(HATT) as shown in Fig. 2-1. Apart from HATT, there are other kinds such as the vertical axis tidal turbine, tidal kite, etc. HATT is more researched and has attracted more investments as compared to any other kind of the tidal turbines [2]. HATT's reliability and survivability in the marine environment are higher than any other tidal generator [2]. Hence we will focus on just HATT.

POD Type or RIM Type

Based on the generator placement within the turbine, tidal turbines can be classified into two configurations i.e. POD type and RIM type. Fig. 2-1a shows an example of POD type generator. In this configuration, the generator is placed behind the turbine blades. Also, the outer diameter of the generator is limited as compared to the blade diameter to avoid blockage of the flow across the blades. In the RIM type, the generator is placed in the shroud surrounding the turbine blades. An example of RIM type generator can be seen in Fig. 2-1b. It must be underlined that the design of such machine is quite

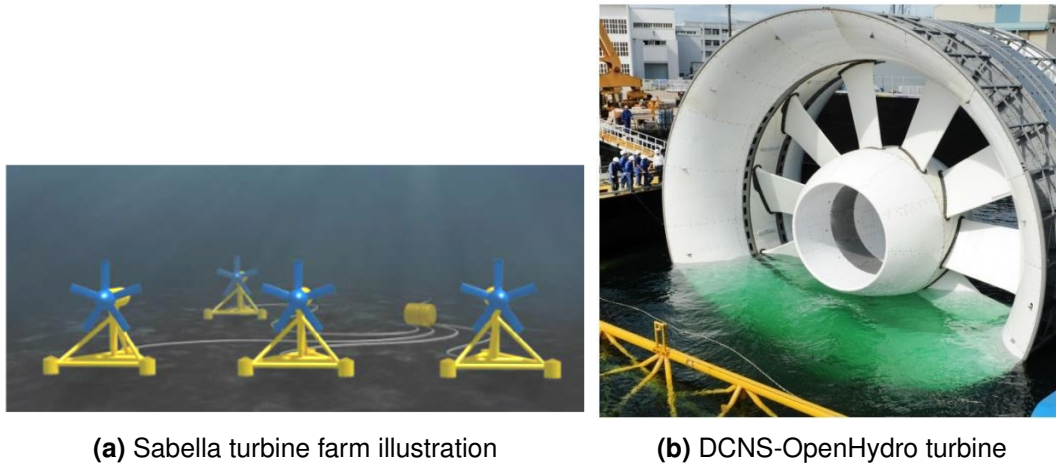


Figure 2-1: Horizontal axis tidal generator [3]

unusual as the active parts of the machine are located at the blade periphery. RIM type generators are more favorable regarding the hydrodynamic efficiency than the POD type. The RIM type generators yield a reduction of about 15% in the cost of active parts as compared to the POD type generator for same turbine specification [21], while the study conducted by Tocardo between 1999 and 2005, suggest that POD type generators are more economical than RIM type generators [2]. But due to the large diameter of the RIM type generators, one of the biggest challenges is the design of economic and reliable bearing system. Hence for further analysis, the POD type generators are considered.

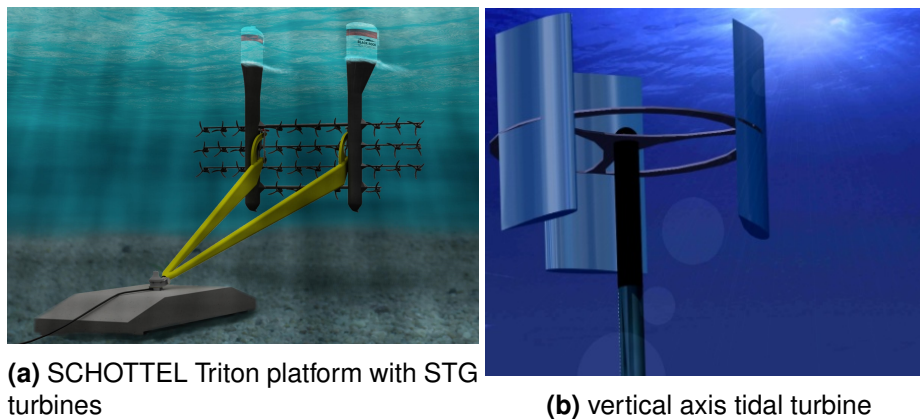


Figure 2-2: Vertical axis tidal generator [2]

Direct Drive Generators or Geared Systems

The conventional industrial generators have higher rotor speed i.e. between 1000rpm to 3000rpm. But due to the relatively low current velocity of the tides, the rotational speed of the turbine is typically below 50rpm to avoid blades cavitation [13]. Due to the difference between the turbine blade velocity and rotor velocity of the generator gearbox must be used, this reduces the reliability and efficiency and also increases the demand for the maintenance. Hence the direct drive permanent magnet generators seem to be the most suitable option for tidal generators [14].

2-3 Analytical Model for Generator Design

The 2D cross-section of the permanent magnet machine is shown in Fig. 2-3, various parameters as indicated in figure are explained in Table 2-1. Geometrical parameter calculation methodology adopted is presented in the following section.

Table 2-1: Geometrical Parameters of the machine

Sr No	Symbol	Description
1	h_{ys}	Stator Yoke thickness
2	h_s	Stator teeth height
3	h_{pm}	Permanent magnet thickness
4	h_{yr}	Rotor yoke thickness
5	h_g	Stator-rotor gap thickness
6	b_m	Permanent magnet Width
7	τ_p	Pole pitch
8	b_d	Teeth thickness
9	b_s	Slot Width
10	c_t	Retaining sleeve thickness

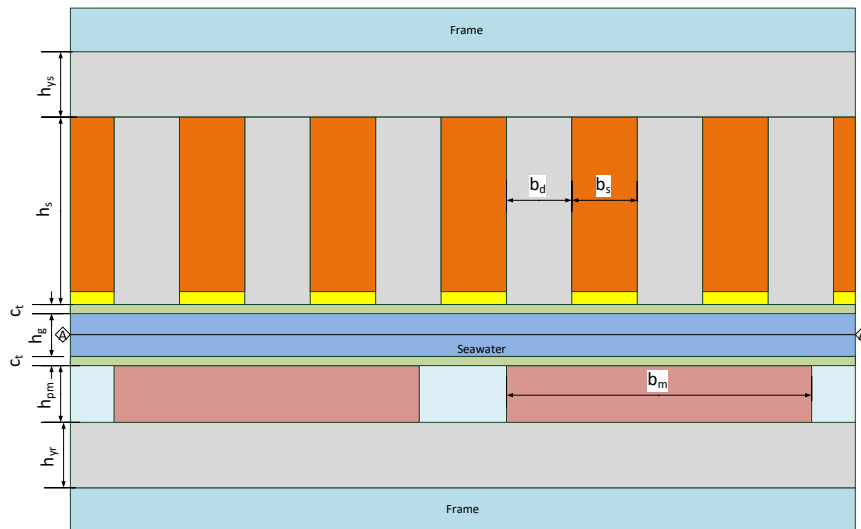


Figure 2-3: Cross section of Rim driven permanent magnet generator [4]

Rotor Diameter

Based on the required power rating of the generator and known stream velocity; the blade radius of the turbine is calculated using the power equation $P = \frac{1}{2}C_p\rho v^3A_u$ [4][14], where ρ is the seawater density, v is the water flow velocity, and A_u is the sweep area of the turbine, the value of the power

coefficient C_p considered is 0.4. The outer radius of the POD type generators is less than 1/6 of the turbine blade radius to avoid blockage of fluid. Based on rated rotor speed, the torque produced by the generator can be calculated by $T = P/\Omega$, where Ω is the angular rotor speed of the rotor. The active length of the machine can be calculated using the equation $T = \sigma_t 2\pi R_r^2 l$, where R_r is the rotor radius, l is rotor equivalent length and σ_t is tangential force density in air gap. The pole pitch $\tau_p = \pi R_r / p$, can be determined using the number of the pole pairs (p) and rotor radius. The total number of slots is $Q = 2pmq$, where q is the number of slots per pole per phase and m is the total number of phases. The slot pitch is $\tau_s = \tau_p / (mq)$ [34][35].

Air Gap

The smallest technically possible air gap is approximately 0.2 mm. In drives for extremely heavy duty, the air gap is increased by 60%. In machines with a large diameter such as direct drive wind turbine and tidal generators, the stator-rotor gap selected is $h_g = 0.002D$ this is because of the mechanical stress of the frame and the shaft of the machine [35].

Coil Turns and Number of Conductor per Slot

The EMF induced (E_{PM}) by the air gap flux linkage ϕ_m can be estimated from the RMS value U_1 the fundamental terminal voltage. In permanent magnet synchronous machines typically, $E_{PM} \approx 0.9 - 1.1U_1$. The peak value of the air-gap flux linkage is given by Equation (2-1), where α_{pm} is the permanent magnet to pole pitch ratio, B_δ is the stator-rotor gap flux density and l is the equivalent length of the rotor [35].

$$\phi_m = \alpha_{PM} B_\delta \tau_p l \quad (2-1)$$

The required number of coil turns N in the phase winding of the machine can be expressed by Equation (2-2), where K_{w1} is winding factor [35].

$$N = \frac{\sqrt{2}E_{PM}}{\omega K_{w1} \phi_m} = \frac{\sqrt{2}E_{PM}}{\omega K_{w1} \alpha_{PM} B_\delta \tau_p l} \quad (2-2)$$

Number of conductors per slot (Z_Q) can be given by Equation (2-3) [35].

$$Z_Q = \frac{2am}{Q} N \quad (2-3)$$

Z_Q has to be an integer. When rounding Z_Q off to an integer, we have to pay attention to the appropriateness of the slot number Q and the number of parallel paths a to avoid too large a rounding-off. After rounding-off, a new number of turns N is calculated for the phase winding [35].

Stator Area

The stator yoke thickness (h_{ys}), the rotor yoke thickness (h_{yr}), and the stator tooth width (b_d) are calculated based on the maximum allowed magnetic flux density. The equations are given as below

[34].

$$h_{ys} = \frac{B_{\delta} \tau_p l_e}{2B_{ys} l_u} \quad (2-4)$$

$$h_{yr} = \frac{B_{\delta} \tau_p l_e}{2B_{yr} l} \quad (2-5)$$

$$b_d = \frac{B_{\delta} \tau_s l_e}{2B_d l_u} \quad (2-6)$$

Where B_{ys} , B_{yr} , and B_d is the maximum allowed no load flux density in the stator yoke, the rotor yoke and the stator teeth respectively. Stator slot area can be calculated based on the stator current and current density by $S_{cs} = (Z_Q I_s) / (k_{cu,s} a J_s)$, where $k_{cu,s}$ is the stator copper fill factor or stator slot space factor. The stator slot and tooth height h_s are always equal. It can be calculated as $h_s = S_{cs} / b_d$. The magnet width is given by $b_m = \alpha_{PM} \tau_p$. The equivalent core length is approximated as $l_e = l + 2h_g$ and useful iron length is $l_u = k_{Fes} l$ where, k_{Fes} is the stator iron fill factor.

Magnet Thickness

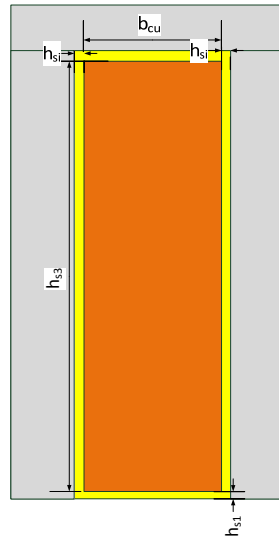


Figure 2-4: The slot and single layer winding

The mmf of the iron core can be calculated from the magnetization curves for the stator and rotor core materials i.e. $H_s(B)$ and $H_r(B)$. In the stator yoke the mmf needed for the magnetic flux between two poles can be approximated as [34]

$$\hat{v}_{ys} = c \left(\tau_p + \frac{\pi(h_s + 0.5h_{ys})}{P} \right) H_s(B_{ys}) \quad (2-7)$$

The mmf needed for the teeth can be expressed approximately as [34]

$$\hat{v}_d = H_s(B_d)(h_{s3} + 0.5h_{s2}) + H_s(B_{\delta})(0.5h_{s2} + h_{s1}) \quad (2-8)$$

The mmf of the rotor yoke is [34]

$$\hat{v}_{yr} = c \left(\tau_p - \frac{\pi(\delta + h_{pm} + 0.5h_{yr})}{P} \right) H_r(B_{yr}) \quad (2-9)$$

Where c takes into account the variation of the field strength in the yoke. For stator and rotor c is assumed to be 0.5. Because h_{pm} is included in this expression, the required magnet height has to be calculated by iteration. The mmf drops \hat{v}_m & \hat{v}_δ of the magnet and air gap are respectively. Where μ_m is the relative permeability of the permanent magnet material.

$$\hat{v}_m = h_{pm} \frac{B_\delta}{\mu_m \mu_0} \quad (2-10)$$

$$\hat{v}_\delta = \delta_{ef} \frac{B_\delta}{\mu_0} \quad (2-11)$$

The sum of the mmf's around the magnetic circuit of two poles is zero [34]

$$2H_c h_{pm} - \hat{v}_{ys} - \hat{v}_{yr} - 2\hat{v}_d - 2\hat{v}_\delta - 2\hat{v}_m = 0 \quad (2-12)$$

Where the H_c is the coercivity of the permanent magnet material. The magnet height can be calculated as follows

$$h_{pm} = \frac{0.5\hat{v}_{ys} + 0.5\hat{v}_{yr} + \hat{v}_d + \hat{v}_\delta}{H_c - \frac{B_\delta}{\mu_m \mu_0}} \quad (2-13)$$

2-3-1 Material Volume and Weight

The volume of different regions can be calculated with following equations. The weight of materials used in the machine can be computed by multiplying the volume by specific weight of the corresponding materials.

$$V_{cu} = 2(l + l_b) Q h_{cu} b_{cu} k_{cu} \quad (2-14)$$

$$m_{cu} = \rho_{cu} V_{cu} \quad (2-15)$$

$$V_{Feys} = l_u \pi (d + 2h_s + h_{ys}) h_{ys} \quad (2-16)$$

$$m_{Feys} = \rho_{Fe} V_{Feys} \quad (2-17)$$

$$V_{Fed} = l_u Q \left(b_d h_{s3} + \frac{(\tau - b_{sl}) + b_d}{2} h_{s2} + (\tau - b_{sl}) h_{s1} \right) \quad (2-18)$$

$$m_{Fed} = \rho_{Fe} V_{Fed} \quad (2-19)$$

$$V_{Feyr} = l \pi (2R_r - 2\delta - 2h_m - h_{yr}) h_{yr} \quad (2-20)$$

$$m_{Feyr} = \rho_{Fe} V_{Feyr} \quad (2-21)$$

$$V_m = 2plb_m h_{yr} \quad (2-22)$$

$$m_m = \rho_m V_m \quad (2-23)$$

Where l_b is end winding length, m_{cu} is weight of copper in stator winding, m_{Feys} is weight of iron in stator yoke, m_{Feyr} weight of iron in rotor yoke, m_m is the permanent magnet weight and ρ_{cu} , ρ_{Fe} , and ρ_m are the density of copper, iron and permanent magnet respectively.

2-4 Losses

2-4-1 Copper Losses

The copper losses at a winding temperature of θ_u can be calculated from the resistivity of the copper $\rho_{cu}(\theta_{cu})$, the RMS current density J_s and the copper volume V_{cu} . The copper losses will be higher if the winding temperature higher and vice versa.

$$P_{cu}(\theta_{cu}) = \rho_{cu}(\theta_{cu}) J_s^2 V_{cu} \quad (2-24)$$

2-4-2 Core Losses

The core losses in the stator and the rotor yoke are due to the hysteresis and the eddy current. Various regions of the machine are exposed to different magnetic flux density amplitudes, waveshapes, and frequencies of excitation hence for calculation of the core loss, the time varying aspect of the magnetic flux, as well as the magnetic flux density characteristics in the different parts of the machine needs to be taken into account. Often, Steinmetz equations are used for core loss calculation based on separation method. Hence eddy current and hysteresis losses are evaluated separately.

Hysteresis occurs as ferromagnetic materials consist of domains, small regions where the magnetic properties of the material are aligned. When the material is not exposed to any external excitation, the domains are arranged randomly such that the net resultant magnetic field of the material is zero. If an external magnetic field is applied to the ferromagnetic material the domains will align according to the magnetic field, however even if the field is removed not all domains will return to their original alignment, and the material becomes slightly magnetized and will stay magnetized unless an external field of the opposite direction is applied. Therefore when an alternating field is applied some extra work needs to be done for every reversal of the field to align all of the domains and losses will, therefore, be induced. This is known as hysteresis loss and is widely estimated by Equation (2-25) for loss per volume [36].

$$P_h = k_h f B^n \quad (2-25)$$

Where k_h is the hysteresis coefficient, which is a constant depending on the material properties and dimension, f is the excitation frequency, B is the flux density and n is the material dependent exponent between 1.5 – 2.5.

Eddy current losses are caused by induced electric currents due to the time-varying magnetic field. These induced eddy currents will circulate locally within the material and power is dissipated as heat due to the resistivity of the material. The eddy current power loss per volume is approximated as shown in Equation (2-26).

$$P_h = k_e f^2 B^2 \quad (2-26)$$

Where k_e is the eddy current coefficient, which is a material-dependent constant. The total core loss in the laminated cores of the electrical machine will be the sum of the hysteresis and eddy current loss components.

2-4-3 Losses in the Permanent Magnets

The rare-earth magnets have relatively low electrical resistivity and low permeability. For low-speed machines the skin depth at the inducing frequencies is significantly greater than both the magnet pole arc and radial thickness of the magnets; hence it can be assumed that the induced eddy current is resistance limited. In Permanent Magnet Synchronous Machine, the fundamental air-gap field rotates in synchronism with the rotor and space harmonics in the winding distribution are small; hence the eddy current losses induced in the permanent magnets are small as compared to core losses. However in fractional slot winding PMSM the lower and higher order space harmonics rotating at different speeds to that of rotor magnets can induce significant eddy current losses in the magnets. The significant temperature rises in PM due to eddy current loss will cause irreversible partial demagnetization.

2-5 Results

Table 2-2 shows the assumed parameters for geometrical parameter calculations for the machine. Higher no of pole pair is considered to reduce the slotting effect. For the design of the machine, conventional materials i.e. NdFeB magnets and FeSi laminations are used. The thicker air gap is chosen to have seawater flow in the air gap. Lower air gap flux density (0.6T) and magnet to pole pitch ratio (0.6) are selected to reduce the amount of the leakage flux. Table 2-3 shows the derived values for integral slot winding. Fig. 3-7 shows the no load magnetic flux density in the center of air-gap calculated analytically, and via FEM. The maximum value of magnetic flux density in air-gap is $0.58T$, while the magnetic flux density in stator teeth and stator yoke are $1.338T$ and $0.602T$ respectively, which are as per the assumptions in Table 2-2. Table 2-4 shows the losses in the tidal generator.

Table 2-2: Assumed variables for the machine

Sr No	Parameter	Symbol	Unit	Assumed value
1	Power rating	P_o	kW	300
2	Rotor speed	Ω	rpm	30
3	Remenant flux density	B_r	T	1.2
4	Air gap flux density	B_δ	T	0.6
5	Maximum tooth flux density	B_d	T	1.6
6	Maximum stator yoke flux density	B_{ys}	T	1.2
7	Maximum rotor yoke flux density	B_{yr}	T	1.2
8	Magnet width to pole pitch ratio	α_{pm}	-	0.6
9	Current Density	J_s	A/mm ²	4
10	Stator iron fill factor	K_{fes}	-	0.9
11	Slot fill factor	$K_{cu,s}$	-	0.8
12	Number of Pole Pair	p	-	70

Table 2-3: Geometric parameters of the Integer slot winding machine

Sr No	Parameter	Symbol	Unit	Configuration-1
1	Slot per pole per phase	q	-	1
2	Rotor internal radius	R_r	m	1.2693
3	Stator length	l	m	0.3706
4	Tooth Width	b_d	mm	7.9
5	Slot Width	b_s	mm	11.1
6	Tooth height	h_s	mm	61
7	Stator-rotor gap	h_g	mm	10
8	PM thickness	h_{pm}	mm	9.6
9	Stator Yoke thickness	h_{ys}	mm	15.8
10	Rotor Yoke thickness	h_{yr}	mm	15

Table 2-4: Losses

Sr No	Loss	Unit	value
1	Iron Loss	kW	1.72
2	Copper Loss	kW	11.63
3	End winding loss	kW	1.78

Fig. 2-5 shows the no-load magnetic flux density in air-gap for various no of pole pairs. As the rotor radius is kept same, for a lower number of poles, the slot opening will be larger than that for a higher number of poles. It can be observed that for a lower number of pole pair the slotting effect is more prominent as compared to the higher number of pole pairs. Hence slotting effect on the magnetic flux density is directly proportional to the slot opening [37]. Fig. 2-6 shows the no load magnetic flux density in a section of the generator. It can be observed that the magnetic flux density in all segments of the machine is within the assumed limits.

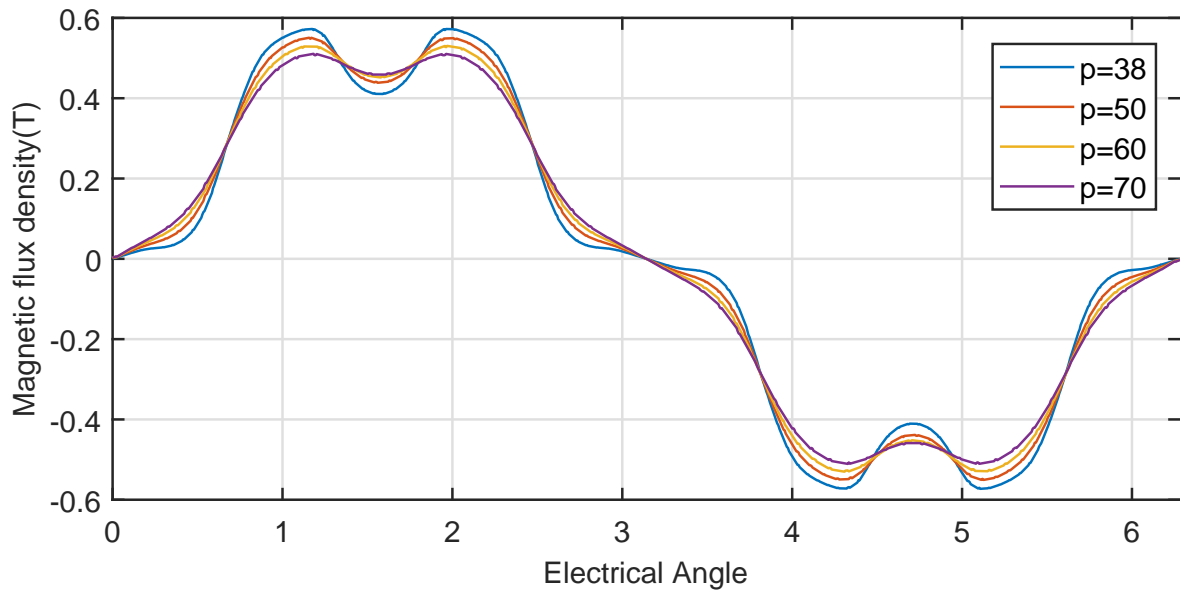


Figure 2-5: Magnetic flux density at A-A position due to different pole pair numbers.

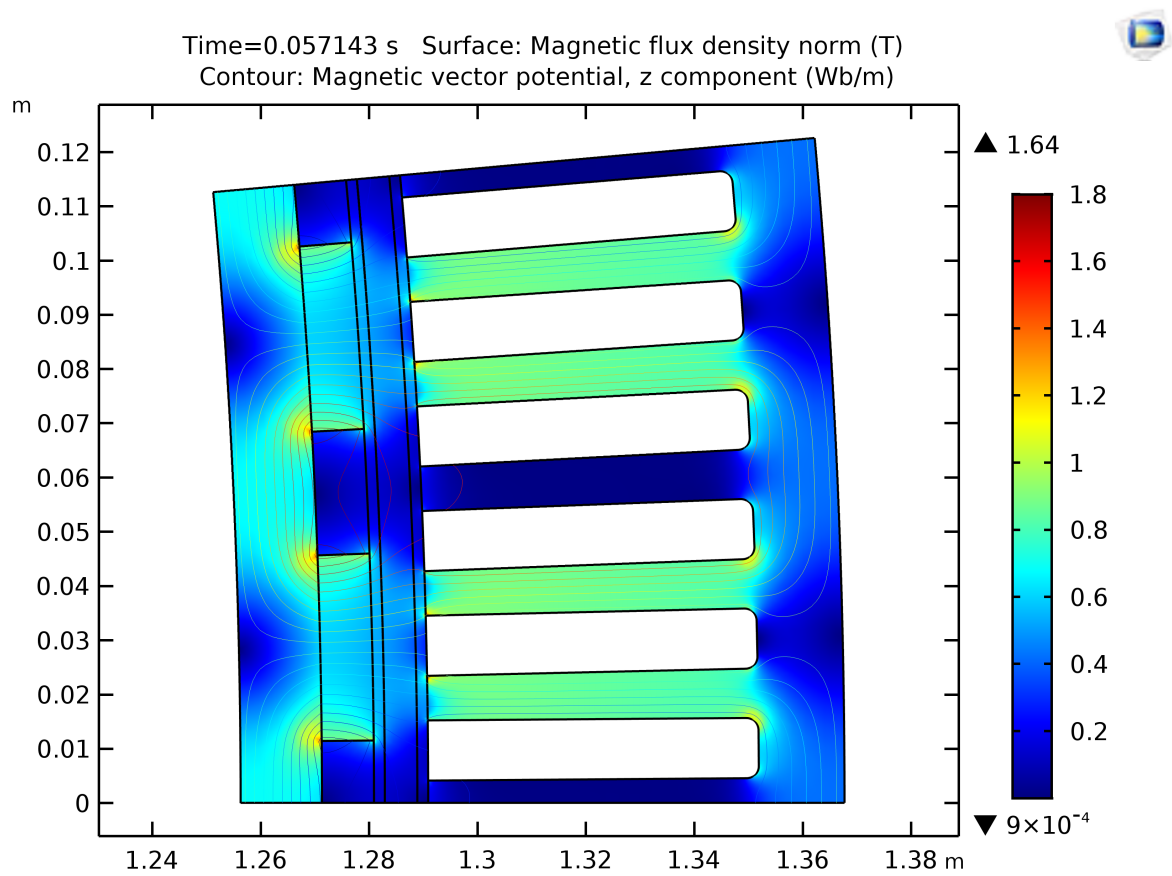


Figure 2-6: FEM result of No load magnetic flux density for integral slot winding machine

Analytical Model for Loss Calculation

3-1 Introduction

The main drawback of the analytical model is that it takes a longer time to initially develop when compared to the finite element model (FEM). Once developed, though, it takes just a fraction of the time to compute as compared to the FEM. The analytical model also gives a better understanding of the problem, by providing powerful insight into the relationship between quantities so that one can quickly see the trends. Such insight is hard to obtain from FEM.

Solving a three-dimensional ($3D$) field analytically is a difficult task and so a two-dimensional ($2D$) approach is adopted. As it is an analytical model that is considered in $2D$, the magnetic field in $3D$ will be ignored; this introduces an error. As the machine can be regarded as flat due to the large diameter, any error derived from neglecting the magnetic field in $3D$ will be quite small. Therefore $2D$ analytical modeling is used for magnetic field calculation and desired values are derived.

In the chapter, firstly, the general governing equation for magnetic vector potential is derived under certain assumptions, based on which magnetic field distributions due to permanent magnets and armature winding are derived. Secondly, eddy current losses in the retaining sleeve are calculated for different materials.

3-2 Mathematical Model

One tool in the analysis and design of a permanent-magnet machine is to be able to predict the magnetic flux density (\mathbf{B}) and field intensity (\mathbf{H}) due to the various field sources in all the machine regions. The problem is formulated in magnetic vector potential as machine inductances, and other parameters can be obtained from the vector potential directly. By using Maxwell equation

$$-\nabla \times \mathbf{H} + \mathbf{J} = -\mathbf{J}_{ext}, \quad (3-1)$$

$$\nabla \times \mathbf{E} + \frac{\partial \mathbf{B}}{\partial t} = 0, \quad (3-2)$$

$$\nabla \cdot \mathbf{J}_{ext} = 0, \quad (3-3)$$

and

$$\nabla \cdot \mathbf{B} = 0. \quad (3-4)$$

The constitutive relations for a linear isotropic medium are:

$$\mathbf{J} = \sigma \mathbf{E} \quad (3-5)$$

Which is ohm's law and

$$\mathbf{B} = \mu \mathbf{H} + \mathbf{B}_{rem} \quad (3-6)$$

Where σ is the conductivity, μ the permeability and B_{rem} is remanent flux density of the material, respectively. By using of Equation (3-1), Ampere's Law (Equation (3-6)) can be rewritten as:

$$\nabla \times \left[\frac{1}{\mu} (\mathbf{B} - \mathbf{B}_{rem}) \right] = \mathbf{J} + \mathbf{J}_{ext} \quad (3-7)$$

$$\nabla \times \frac{1}{\mu} \mathbf{B} = \mathbf{J} + \mathbf{J}_{ext} + \left(\nabla \times \frac{1}{\mu} \mathbf{B}_{rem} \right) \quad (3-8)$$

Since \mathbf{B} is solenoidal from Equation (3-4), it can be written in terms of the vector potential as:

$$\mathbf{B} = \nabla \times \mathbf{A} \quad (3-9)$$

$$\mathbf{E} = -\frac{\partial \mathbf{A}}{\partial t} \quad (3-10)$$

By substituting Equations (3-9), (3-10), (3-5) into Equation (3-8) the result is

$$-\nabla^2 \mathbf{A} + \mu \sigma \frac{\partial \mathbf{A}}{\partial t} = \mu \mathbf{J}_s + \nabla \times \mathbf{B}_{rem} \quad (3-11)$$

Where the external current density \mathbf{J}_{ext} has been replaced by the stator current density \mathbf{J}_s . The Equation (3-11) relates the vector potential (including the eddy current effect on it) to the two main fields sources in the machine: the permanent magnet array described by \mathbf{B}_{rem} , and the stator current density described by \mathbf{B}_s .

For solving the Equation (3-11) several assumptions needs to be made, which are

1. The magnetic vector potential is linear i.e. potential of different sources can be simply added algebraically i.e. $\mathbf{A}_{total} = \mathbf{A}_{magnets} + \mathbf{A}_{statorCurrents}$, and have symmetry i.e., $\mathbf{A}(r, \theta) = -\mathbf{A}(r, \theta + \frac{\pi}{p})$
2. The vector potential has only z -component and it is dependent on only r and θ .
3. The relative permeability of the stator and rotor iron is infinite (∞) i.e. it does not saturate while relative permeability of all non-iron part is equal to 1.
4. All material are linear and isotropic.
5. The magnets do not demagnetize.

3-3 Boundary Conditions

The boundary condition implied by Ampere's Law states that the tangential component of the magnetic field intensity on one side of the boundary is equal to that of the other side plus a surface current density,

$$\hat{\mathbf{n}} \times (\mathbf{H}^1 - \mathbf{H}^2) = \mathbf{K} \quad (3-12)$$

where $\hat{\mathbf{n}}$ is the unit normal vector, \mathbf{H}^1 and \mathbf{H}^2 denotes the magnetic field intensity in region 1 & 2 respectively and \mathbf{K} the surface current density at the boundary interface between regions 1 and 2. The boundary condition implied by the magnetic flux conservation law states that the normal component of the flux density on one side of a boundary is equal to that on the other side, or mathematically:

$$\hat{\mathbf{n}} \cdot (\mathbf{B}^1 - \mathbf{B}^2) = 0 \quad (3-13)$$

3-4 Skin Depth

At high frequencies, the tendency of the electric current is to flow in the outer layer of the conductor from the even distribution of current at the lower frequency this is known as skin effect. The skin effect causes the effective resistance of the conductor to increase at high frequencies when the skin depth is smaller. The skin depth can be given by:

$$\delta = \sqrt{\frac{2}{\omega\sigma\mu}} \quad (3-14)$$

where ω is the angular frequency, σ is the conductivity of the material and μ is the permeability. The skin depth for various materials at different harmonic order is shown in Fig. 3-1 when rotor speed is 30rpm. Due to slow speed, relatively high resistivity and low permeability of the retaining sleeve and magnets, the skin depth for the dominant harmonics i.e. (5th, 7th, 11th, 13th, etc) is greater than the thickness of the region. Hence the influence of the skin effect can be neglected.

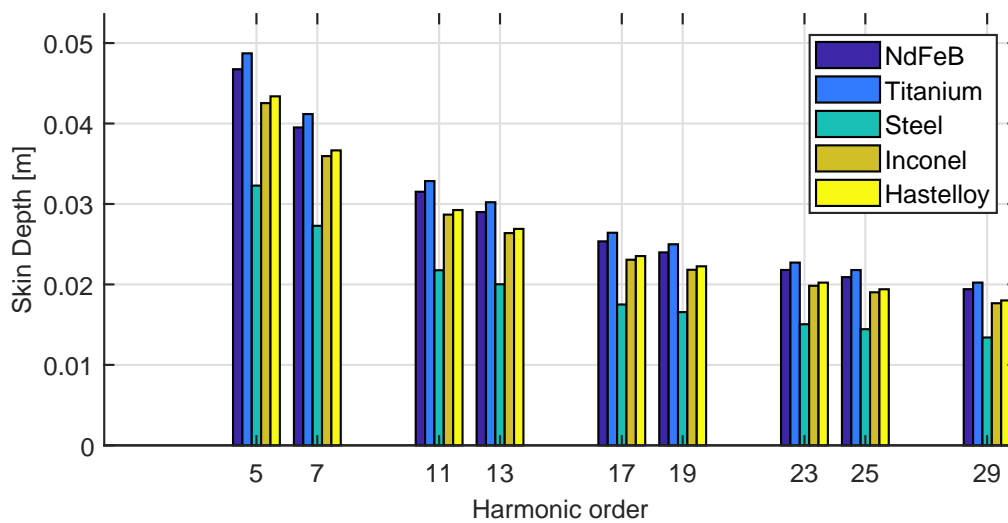


Figure 3-1: Skin depth calculated at different harmonic order

3-5 Magnetic Field due to Magnets

For the derivation of magnetic vector potential A due to radial permanent magnets, the governing Equation (3-11) can be further simplified by making following assumptions.

- The eddy current effects upon A are neglected as the skin depth is greater the thickness and width of the magnet.
- As we are considering the field due to magnets only. The stator current density is also set to zero. i.e. $J_s = 0$

This simplifies the Equation 3-11 to as follows.

$$-\nabla^2 A = \nabla \times B_{rem}, \quad (3-15)$$

$$\frac{\partial^2 A}{\partial r^2} + \frac{1}{r} \frac{\partial A}{\partial r} + \frac{1}{r^2} \frac{\partial^2 A}{\partial \theta^2} = -\frac{B_{rem,\theta}}{r} - \frac{\partial B_{rem,\theta}}{\partial r} + \frac{1}{r} \frac{\partial B_{rem,r}}{\partial r}. \quad (3-16)$$

Table 3-1: Machine regions defined for calculating the vector potential from Equation (3-15)

Sr. No	Description	μ_r	Governing Equation
1	Stator iron region	∞	$-\nabla^2 A = 0$
2	Winding region & mechanical airgap region	1	$-\nabla^2 A = 0$
3	Permanent magnet region	1	$-\nabla^2 A = \nabla \times B_{rem}$
4	Rotor iron region	∞	$-\nabla^2 A = 0$

Table 3-1 lists the machine regions within which Equation (3-16) is solved for A . For simplification, an assumption can be made that only remnant radial component of flux density is present and tangential component is zero. Therefore, the remnant flux density of the magnets can be described by the vector.

$$B_{rem} = \begin{cases} B_{rem,r} \hat{r} & \text{North pole magnet} \\ -B_{rem,r} \hat{r} & \text{South pole Magnet} \\ 0 & \text{otherwise} \end{cases} \quad (3-17)$$

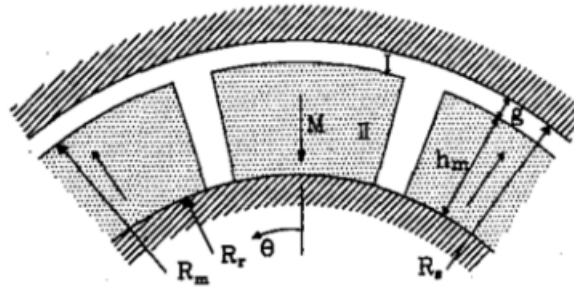


Figure 3-2: Cross section of slot less internal rotor machine [5]

Based on the Fig. 3-2 and the boundary condition as given in 3-18 to 3-21, the radial magnetic flux density in the mechanical airgap can be given by Equation (3-22) [5].

$$H_{\theta I}(r, \theta)_{r=R_s} = 0 \quad (3-18)$$

$$H_{\theta II}(r, \theta)_{r=R_r} = 0 \quad (3-19)$$

$$B_{rI}(r, \theta)_{r=R_m} = B_{rII}(r, \theta)_{r=R_m} \quad (3-20)$$

$$H_{\theta I}(r, \theta)_{r=R_m} = H_{\theta II}(r, \theta)_{r=R_m} \quad (3-21)$$

$$B_{rI}(r, \theta) = \sum_{n=1,3,5,\dots}^{\infty} \frac{\mu_0 M_n}{\mu_r} \frac{np}{(np)^2 - 1} \left\{ \frac{(np-1) \left(\frac{R_m}{R_r}\right)^{2np} + 2 \left(\frac{R_m}{R_r}\right)^{np-1} - (np+1)}{\frac{\mu_r+1}{\mu_r} \left[1 - \left(\frac{R_s}{R_r}\right)^{2np}\right] - \frac{\mu_r-1}{\mu_r} \left[\left(\frac{R_s}{R_m}\right)^{2np} - \left(\frac{R_m}{R_r}\right)^{2np}\right]} \right\} \left[\left(\frac{r}{R_m}\right)^{np-1} - \left(\frac{R_s}{R_m}\right)^{np-1} \left(\frac{R_s}{r}\right)^{np+1} \right] \cos(np\theta) \quad (3-22)$$

Where R_r , R_m , and R_s are the rotor yoke, permanent magnet surface, and stator yoke radii respectively, p is the number of pole pairs, and

$$M_n = \left(\frac{2B_r \alpha_{pm}}{\mu_0} \right) \frac{\sin\left(\frac{n\pi\alpha_{pm}}{2}\right)}{\frac{n\pi\alpha_{pm}}{2}}$$

where B_r is the remanent flux density of magnet and α_{pm} is the magnet width to pole pitch ratio. Fig. 3-3 shows the magnetic flux density derived at the center of the stator-rotor gap as shown in Fig. 2-3 (position A-A) based on the Equation (3-22) for the integral slot winding machine with parameters as mentioned in Table 2-3. The corners of the flux density in Fig. 3-3 are rounded due to the fringing effect. The fringing effect is a phenomenon in which the corners of the flux density in the air gap due to the magnets become rounded and the flat top becomes narrower. The fringing effect also decreases the mean air gap flux density per pole [37].

3-6 Current Sheet Distribution

For simplification purpose, the stator winding is represented by an equivalent current sheet at the outer surface of stator teeth. The current density distribution due to a single conductor can be represented by Equation (3-23). Fig. 3-4 shows an distribution of current due to one winding.

$$J_s = \begin{cases} \frac{i}{b_o} & -\frac{b_o}{2R_s} \leq \alpha \leq \frac{b_o}{2R_s} \\ 0 & \text{otherwise} \end{cases} \quad (3-23)$$

3-7 Magnetic Flux due to Armature Winding

The magnetic vector potential due to armature winding can be derived by modifying the governing equation (3-11) with following assumptions

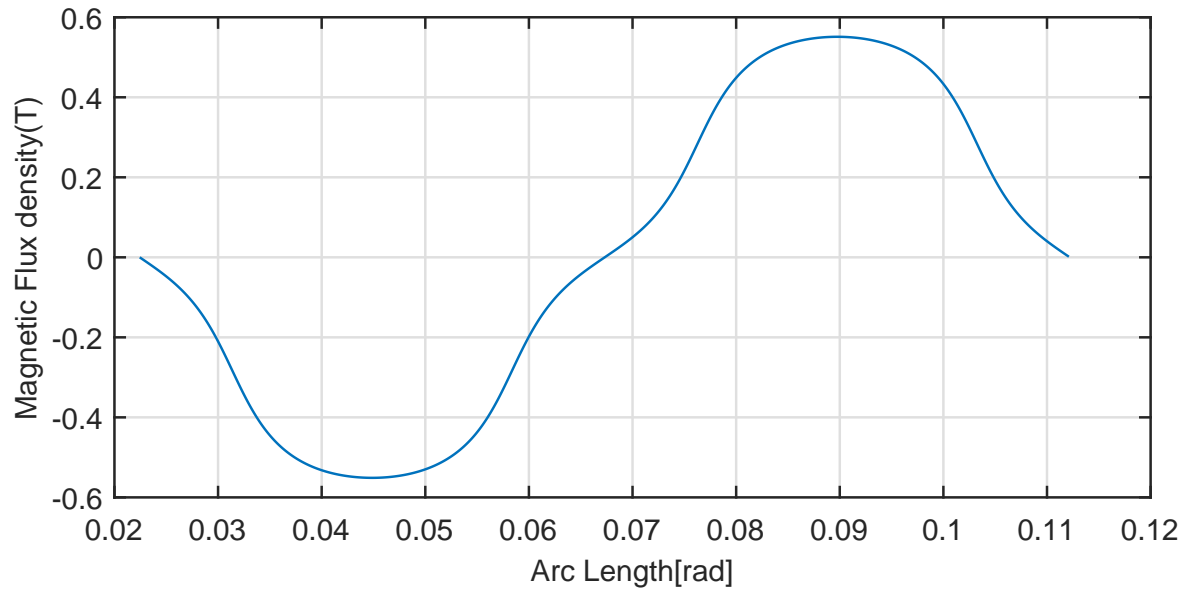


Figure 3-3: Radial magnetic flux density due to the PM for slotless machine derived at the center of the stator-rotor gap.

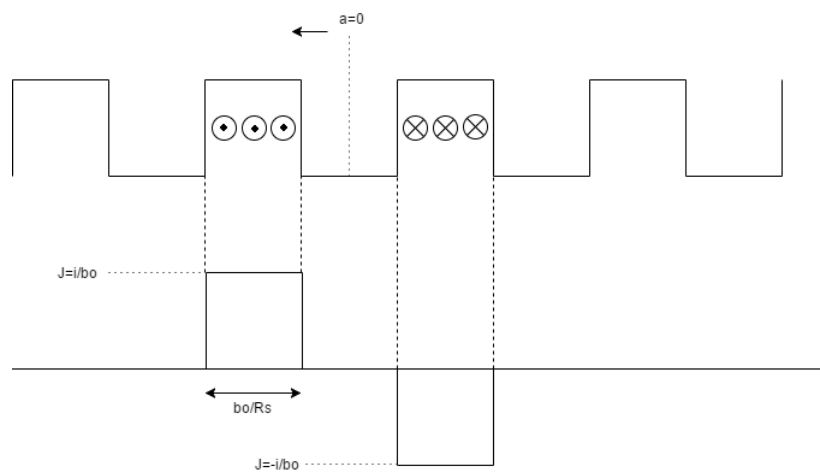


Figure 3-4: Current Density due single winding

1. Permanent magnet excitation is set to zero i.e. $B = 0$
2. As the skin depth is higher than the thickness of the retaining sleeve and the PM. The eddy current can be set to zero.

$$-\nabla^2 A = 0 \quad (3-24)$$

Laplace Equation (3-24) becomes the governing equation in all regions of the machine if we use the current sheet distribution. After solving the Laplace equation considering the boundary conditions, the radial component of the magnetic flux for a single coil is

$$B(\alpha, r) = \frac{2\mu_0 i}{\pi \delta} \sum_v \frac{1}{v} k_{sov} k_{pv} F_v(r) \cos(v\alpha) \quad (3-25)$$

Where

- $k_{pv} = \sin\left(\frac{v\alpha_y}{2}\right)$ is the winding pitch factor. α_y is the winding pitch.
- $\delta = h_g + h_{pm}$ is the effective air-gap.
- $k_{sov} = \frac{\sin\left(v\frac{b_o}{2R_s}\right)}{v\frac{b_o}{2R_s}}$ is the slot opening factor
- $F_v(r) = \delta \frac{v}{r} \left(\frac{r}{R_s}\right)^v \left[\frac{1 + \left(\frac{R_r}{r}\right)^{2v}}{1 - \left(\frac{R_r}{R_s}\right)^{2v}} \right]$ is a function dependent on the radius and harmonic order.

A winding distribution factor k_{dv} is introduced to obtain field due to distributed phase winding. When the q slot per phase per pole is integral, k_{dv} is given by:

$$k_{dv} = \frac{\sin\left(q\frac{v\pi}{Q_s}\right)}{q\sin\left(\frac{v\pi}{Q_s}\right)} \quad (3-26)$$

The magnetic flux density due to 3 phase winding can be deduced by adding all phases as given below

$$B_{winding}(\alpha, r, t) = B_a(\alpha, r, t) + B_b(\alpha, r, t) + B_c(\alpha, r, t) \quad (3-27)$$

$$B_{winding}(\alpha, r, t) = \mu_0 \frac{2W}{\pi\delta} \sum_v \frac{1}{v} k_{sov} k_{pv} F_v(r) \left[i_a \cos(v\alpha) + i_b \cos v\left(\alpha - \frac{2\pi}{3p}\right) + i_c \cos v\left(\alpha - \frac{4\pi}{3p}\right) \right] \quad (3-28)$$

The harmonic order associated with stator winding can be given as

$$v = \begin{cases} p(6c - \{\pm\}u) & \text{for an overlapping winding} \\ p(3c - \{\pm\}u) & \text{for a non overlapping winding} \end{cases} \quad (3-29)$$

Hence two-dimensional radial magnetic flux density can be arrived by simplifying the Equation 3-28 while considering Equation 3-29 to give:

$$B_{winding}(\alpha, r, t) = \mu_0 \frac{3W}{\pi\delta} \sum_u I_u \sum_v \frac{1}{v} k_{sov} k_{dpv} F_v(r) \sin(up\omega_r t \pm v\alpha + \theta_u) \quad (3-30)$$

Fig. 3-5 shows the magnetic flux density at the center of the stator-rotor gap as shown in Fig. 2-3 (position A-A) due to slotless machine computed with Equation 3-30.

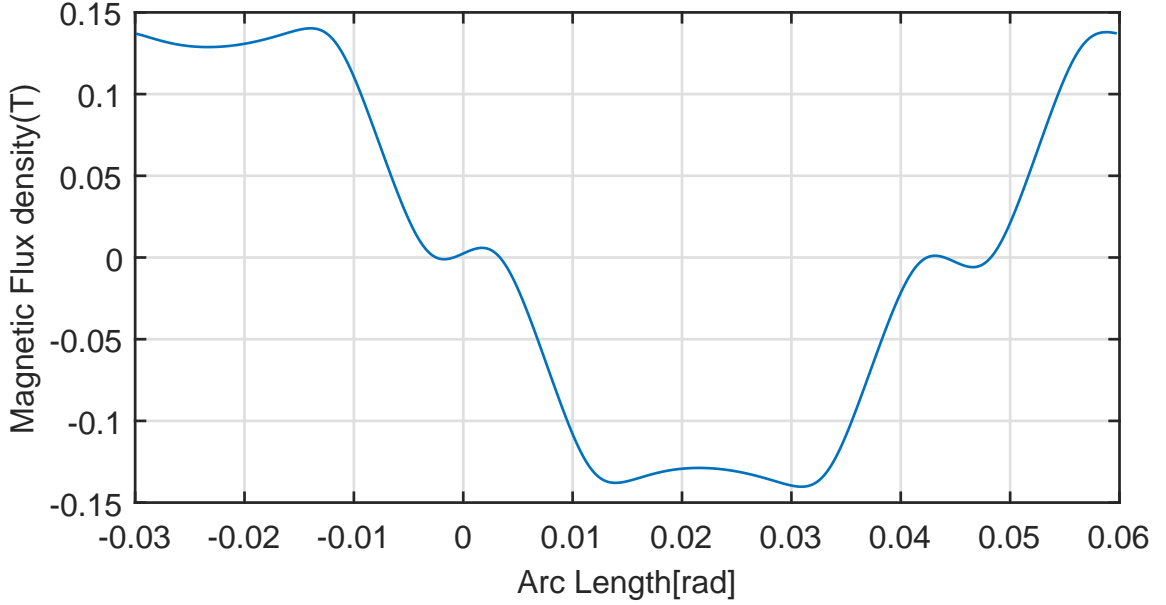


Figure 3-5: Magnetic flux density due to the armature winding for slotless machine derived at the center of the stator-rotor gap.

3-8 Effect of Stator Slotting

To consider the effect of stator slotting a relative permeance function is considered based on the approach of Zhu and Howe [6]. The relative permeance function is calculated by conformal transformation assuming infinitely deep rectilinear stator slot as shown in Fig. 3-6.

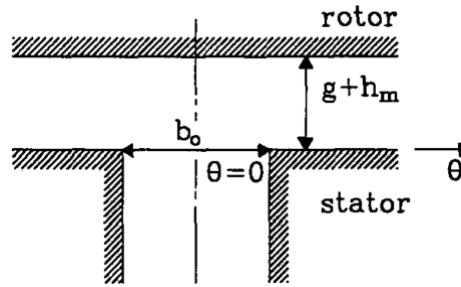


Figure 3-6: Permeance calculation model [6]

The permeance function expressed in the form of Fourier series is as below.

$$\tilde{\lambda}(\alpha, r) = \sum_{\mu=0}^{\infty} \tilde{\Lambda}_{\nu}(r) \cos \nu Q_s (\alpha + \alpha_{sa}) \quad (3-31)$$

The angle α_{sa} is required to align permeance function with the axis of phase A coil. The α_{sa} depends on the winding pitch being odd or even multiple of the stator slot [38].

$$\alpha_{sa} = \begin{cases} \text{half pole pitch} = \frac{\pi}{Q_s} & \text{Winding Pitch is odd integer of the slot pitch} \\ 0 & \text{Winding Pitch is even integer of the slot pitch} \end{cases} \quad (3-32)$$

The Fourier coefficient of the permeance function is given as

$$\tilde{\Lambda}_v(r) = \begin{cases} \frac{1}{K_c} \left(1 - 1.6\beta \frac{b_o}{\tau_r}\right) & \text{when } v = 0 \\ -\beta(r) \frac{4}{\pi v} \left[0.5 + \frac{(v \frac{b_o}{\tau_r})^2}{0.78125 - 2(v \frac{b_o}{\tau_r})^2}\right] \sin\left(1.6\pi v \frac{b_o}{\tau_r}\right) & \text{when } v \neq 0 \end{cases} \quad (3-33)$$

Where K_c is Carter factor which expresses the reduction in the flux per pole due to slotting. The function $\beta(r)$ is deduced from conformal transformation and is given by

$$\beta(r) = \frac{1}{2} \left[1 - \frac{1}{\sqrt{1 + \left(\frac{b_o}{2\delta}\right)^2 (1 + v^2)}} \right] \quad (3-34)$$

Where v is determined by solving the following equation

$$y \frac{\pi}{b_o} = \frac{1}{2} \ln \left[\frac{\sqrt{a^2 + v^2} + v}{\sqrt{a^2 + v^2} - v} \right] + \frac{2\delta}{b_o} \arctan \frac{2\delta}{b_o} \frac{v}{\sqrt{a^2 + v^2}} \quad (3-35)$$

3-9 Slotted Machine Results

The field due to the stator winding and permanent magnet is the product of the field computed due to the slotless machine and relative permeance function:

$$B_{pm}(\alpha, r, t) = B_{pm-slotless}(\alpha, r, t) \tilde{\lambda}(\alpha, r) \quad (3-36)$$

$$B_{armature}(\theta, r, t) = B_{armature-slotless}(\alpha, r, t) \tilde{\lambda}(\alpha, r) \quad (3-37)$$

Where $\alpha = \theta + \omega_r t$ transform the field distribution from stationary coordinate system α to rotating reference frame θ . Fig. 3-7 shows magnetic flux density for a slotted machine at the center of the stator-rotor gap due to the permanent magnet. Fig. 3-8 shows the magnetic flux density due to the armature winding at the A-A position in the stator-rotor gap. It can be observed that the field derived analytical and FEM are in good agreement with each other with an error of less than 5% in magnitude.

3-10 Retaining Sleeve Material

In the case of flooded machines, the permanent magnets need to be separated from water with an insulating layer/sleeve to protect magnets from corrosion. In the case of a high-speed machine, the sleeve is provided on top of the magnets to protect it from cracking due to high centrifugal force at high speed. Hence it is important for the sleeves to have high tensile strength with minimal electrical conductivity. The insulating sleeve is also known as retaining sleeve for a high-speed machine.

The sleeves can be of a metallic and a non-metallic material, Table 3-2 lists the popular materials used in high-speed machines as retaining sleeve [22],[23], [39]. All metallic material selected are non-magnetic are corrosion proof.

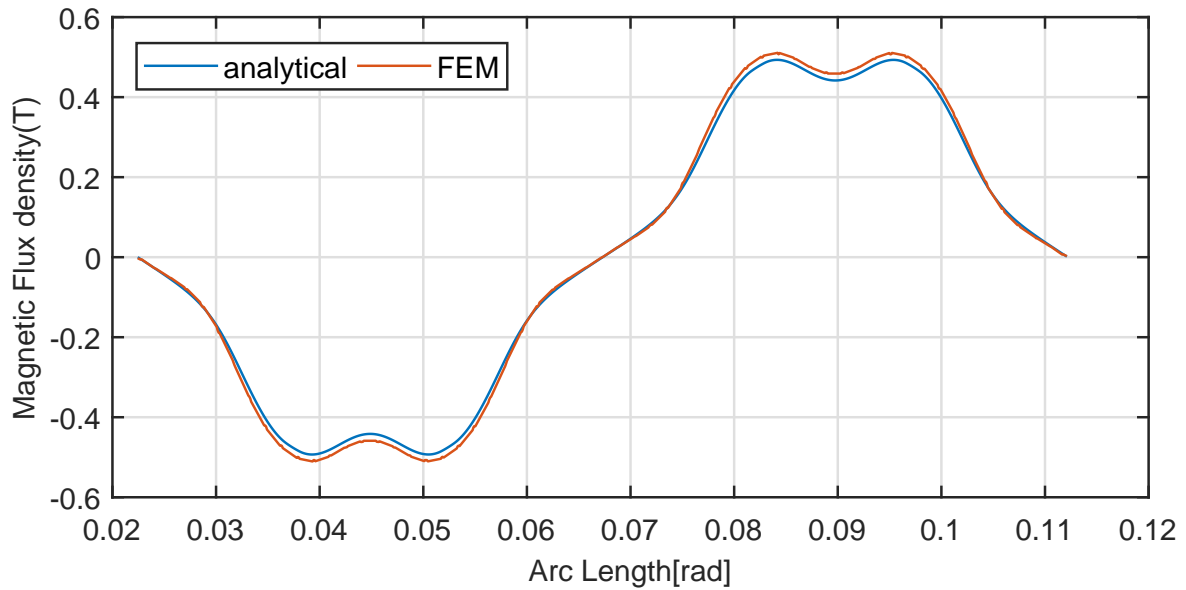


Figure 3-7: Analytical PM field(slotted)vs FEM field

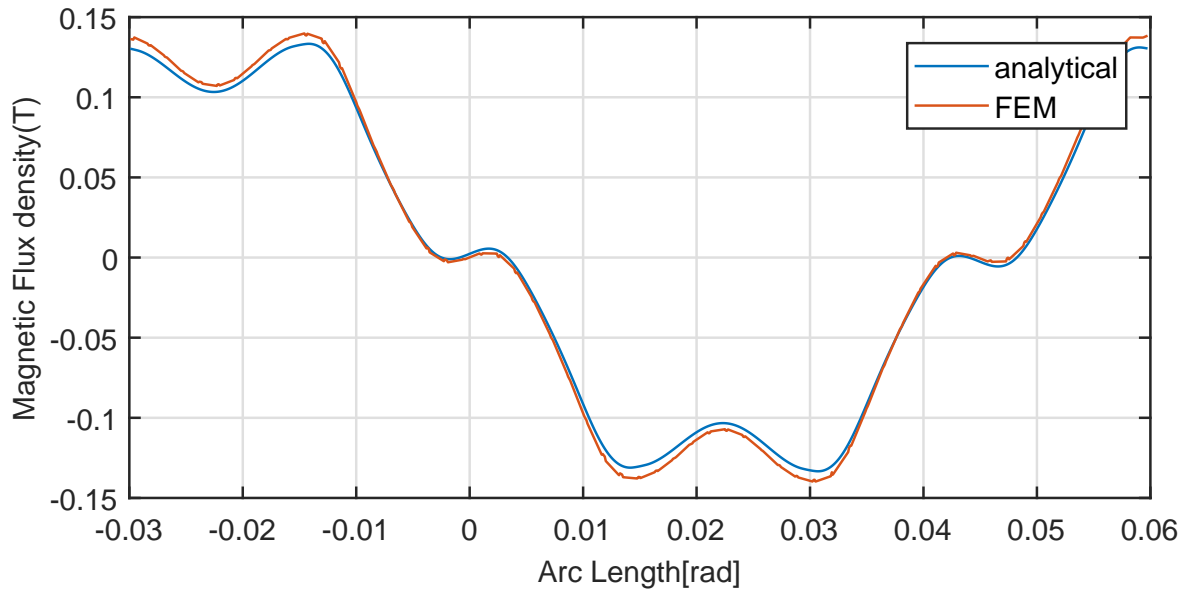


Figure 3-8: Analytical armature winding field(slotted)vs FEM field

Table 3-2: Different materials used as insulation material

Name of material	Unit	Austenitic Stainless steel (304L)	Hastelloy C-276 alloy	Epoxy/Carbon Fiber Composite	Carbon Fiber Filled (PTFE)	Inconel Alloy 718	Titanium (SP700)	Copper
Electrical resistivity	$\Omega - \text{mm}^2/\text{m}$	0.72	1.30	1.30×10^{17}	1.00×10^{11}	1.25	1.64	0.02
Electrical conductivity	MS/m	1.39	0.77	0.00	0.00	0.80	0.61	58.82
Thermal Conductivity	$\text{W}/\text{m} - ^\circ\text{C}$	16.20	10.20	400	0.99	11.40	7	398
Tensile Strength	Mpa	586	792	3,790	28	1,100	960	210
Density	kg/m^3	8,030	8,890	2,250	2,650	8,190	4,544	8,930
Magnetic permeability	-	1.02	-	-	-	1.00	1.00	1.00

A study conducted in [40] suggest that composite non-magnetic materials such as GRP are water absorbing in nature. Seepage of water into sleeve material will cause electrical breakdown of the material over time due to change in electrical permittivity. Hence for further study, non-metallic materials are not considered. Retaining sleeves can be used in two different configurations as shown in Fig. 3-9. In configuration-1 only one type of material is used while in configuration-2 two materials are used, i.e., Copper (0.5mm) and other material (1.5mm).

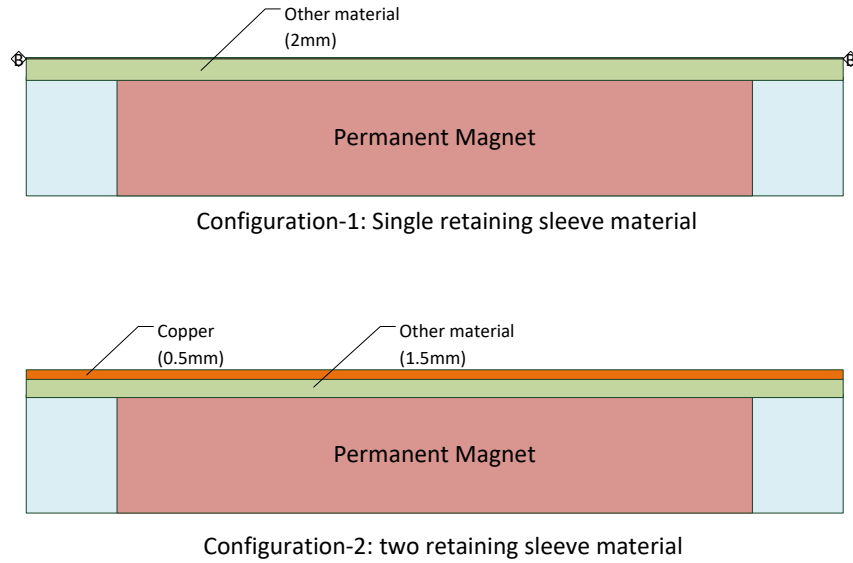


Figure 3-9: Retaining sleeve configurations

3-11 Eddy Current Induced in the Retaining Sleeve

The relation between the magnetic field and induced eddy current is given by:

$$J_z = -\sigma \int \frac{\partial B(\theta, r)}{\partial t} r d\theta \quad (3-38)$$

Where $B(\theta, r)$ is the radial component of the field distribution in the retaining sleeve, and σ is the associated electrical conductivity. The resultant eddy current loss is determined by [41] [24]:

$$P = \frac{2p}{T} \int_0^T \int_0^L \int_{-\alpha_p \pi/2}^{\alpha_p \pi/2} \int_{R_1}^{R_2} \frac{J_z^2}{\sigma} r dr d\theta dz dt \quad (3-39)$$

Where $T = 2\pi/\omega_r$, and $T = 2\pi/\omega_r$, L is the axial length of the rotor, R_1 and R_2 are the inner and outer radii of the retaining sleeve. Fig. 3-10 shows the induced current density at the B-B position (Fig. 3-9) in the rotor retaining sleeve for Inconel material.

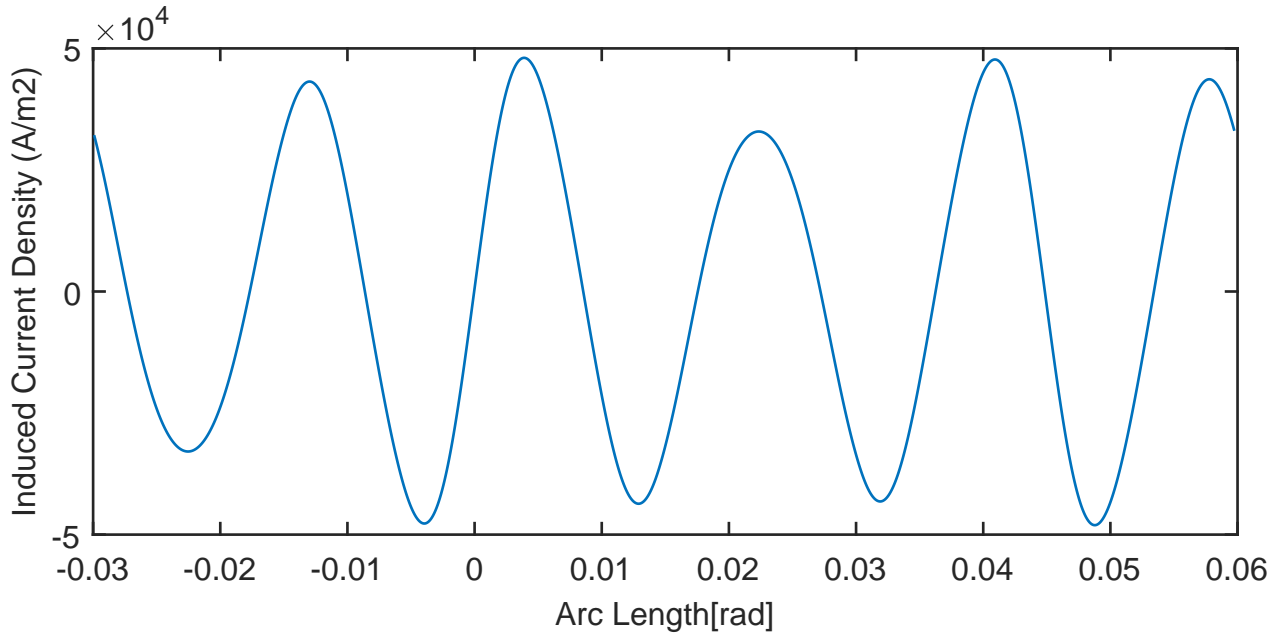


Figure 3-10: Induced Current density in rotor retaining sleeve at outer radii (B-B position) for Inconel material.

3-12 Results

Table 3-3 shows the eddy current losses in the permanent magnet, rotor retaining sleeve calculated analytically and FEM. It can be observed that that error in the loss calculated is less than 10%. There is also a reduction in PM loss when retaining sleeves are used. The decrease in PM loss is due to shielding effect provided by retaining sleeve. The shielding effect is also small in this configuration because of difference in the electrical conductivity of the retaining sleeve, and the PM is small.

Table 3-3: Eddy current losses for various rotor retaining sleeve material

Sr No	Retaining sleeve material	Permanent magnet Eddy current loss(W)	Retaining sleeve Eddy current loss(W) (Analytical)	Retaining sleeve Eddy current loss(W) (FEM)
1	No retaining sleeve	3.54	-	-
2	Inconel	3.44	14.74	13.55
3	Steel	3.37	25.61	23.74
4	Hastelloy	3.45	14.81	13.05
5	Titanium	3.47	11.23	10.34

Table 3-4 shows the eddy current loss in the stator retaining sleeve for various materials; it can be observed that the losses are higher than the losses in the rotor retaining sleeve and iron and copper losses as given in Table 2-4. Higher losses in stator sleeve are due to two primary reasons, firstly the stator retaining sleeve is stationary with reference to the rotating magnetic flux density. Secondly proximity of the stator sleeve with the stator teeth, due to this the stator sleeve experience higher spatial harmonics.

Table 3-4: Eddy current losses in stator retaining sleeve for various material

Sr No	Retaining sleeve material	Stator retaining sleeve Eddy current loss(W)
1	Inconel	12295
2	Steel	21478
3	Hastelloy	11840
4	Titanium	9381.8

FEM Results

As the analytical model developed does not consider the skin effect, the shielding effect can not be observed when we use two different materials. Hence to calculate the eddy current losses for the copper sleeve and other materials FEM model is used. Table 3-5 shows the eddy current losses in the rotor retaining sleeve when configuration-2 is used. As the thickness of the copper layer smaller than the skin depth, skin effect can be observed at the outer radii.

Table 3-5: Eddy current losses in rotor retaining sleeve for Integral slot winding machine

Sr No	Retaining sleeve material	Permanent magnet Eddy current loss(W)	Retaining sleeve Eddy current loss(W)	Copper sleeve Eddy current loss(W)
1	Inconel	4.06	12.78	520.8
2	Steel	4.05	22.15	519.62
3	Hastelloy	4.06	12.30	520.59
4	Titanium	4.07	9.75	520.84

3-13 Conclusion

The eddy current loss in the stator sleeve is higher than the total copper and iron loss of the machine. Therefore the use of an electrically conductive material in stator sleeve is of disadvantage. For rotor sleeve, configuration-1 should be used due to two reason. First, the eddy current losses increase by ten times when a copper sleeve is used. Second, the copper is prone to corrosion from seawater when used on outer radii while at inner radii it will be near to PM and will increase the temperature of the PM.

Chapter 4

Magnetohydrodynamics

4-1 Introduction

Magnetohydrodynamics (MHD) is a scientific branch for studying the dynamics of the fluid motion in the presence of an electromagnetic field. In the case of an electrically conductive fluid, the induced current modifies the magnetic field, and the forces influence the motion of the fluid [42]. In the case of marine current turbines or tidal generators, the stator-rotor gap is filled with seawater which is electrically conductive. The MHD phenomena will be induced in the stator rotor gap due to rotating magnetic flux density. The MHD will lead to additional losses and flow distortion in the stator-rotor gap [33]. This non-conventional phenomenon is often neglected in the designing process as the MHD losses are assumed to be negligible due to a very low electrical conductivity of seawater. But it is important to analyze these losses and see the overall significance.

The chapter will firstly discuss the fluid flow between two concentric cylinders. Secondly, a model is developed to evaluate fluid velocity in stator-rotor gap. Thirdly MHD losses in the stator-rotor gap are evaluated.

4-2 Taylor - Couette Flow

Fig. 4-1 is a representation of an electrical machine's stator-rotor gap and direction of seawater flow in the gap. The inner cylinder of radius R_i is rotating at a given rotation rate Ω , while the outer cylinder of radius R_o is stationary. This configuration in literature is known as the Taylor – Couette problem. The length of the machine is denoted as h . An axial volume flow rate Q can be superimposed at the cavity inlet [7]. The rotational Reynolds number Re_i based on the rotating speed of the inner cylinder ΩR_i and half the hydraulic diameter $\Delta R = (R_o - R_i) / Ri$ and the flow rate coefficient $C_w = Q / (vR_o)$.

$$Re_i = \frac{\Omega R_i (R_o - R_i)}{\nu} \quad (4-1)$$

Where $\nu = 1.83 \times 10^{-6} (m^2/s)$ is the kinematic viscosity of seawater at $0^\circ C$.

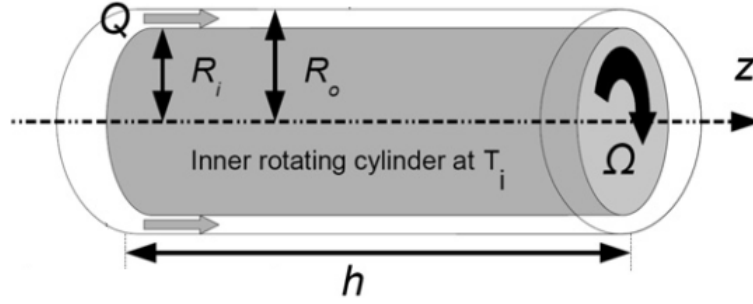


Figure 4-1: Schematic representation of the Taylor-Couette-Poiseuille configuration with relevant notations [7]

If Reynolds number is less than the critical value of 1700, then the fluid flow is termed as laminar flow else it is a turbulent flow. Table 4-1 shows the Reynolds number calculated for three different configurations. The fluid flow in configuration-2 & 3 are turbulent while configuration-1 is laminar. In this thesis, we will limit our analysis to laminar flow to avoid complex modeling of turbulent flow.

Table 4-1: Reynolds number calculated for different machine dimension

	$R_i(m)$	stator rotor gap (mm)	$\Omega(rpm)$	R_{ei}
Configuration-1	1	1	15	858
Configuration-2	1.2809	6	15	6596.8
Configuration-3	1.2809	6	30	13149

4-3 The MHD Model

For the modeling of the MHD model following assumptions are considered.

1. The magnetic field density is oriented in the radial direction only and the magnetic flux density (MFD) rotates at a rotor speed $\Omega = \omega/p$.
2. The End effects are neglected.
3. The air-gap fluid flow is in the azimuthal direction, with the angular speed $\Omega_f(r)$ depending only on the radial position r (laminar flow).

The expression for the radial magnetic flux density in cylindrical coordinate is given by $B_r(r, \theta, t) = B_m \sin(p[\Omega - \Omega_f(r)]t - p\theta)$ [33], where B_m is the MFD magnitude and θ is the angular position. The electric field E and the current density J are induced in the conductive fluid due to the variation of the MFD. It is assumed that the induced electric field and induced current density has only z component. The magnetic field generated by the induced current in the fluid is neglected as B_m is much higher than the induced magnetic field in the fluid. From Maxwell-Faraday's law

$$\frac{1}{r} \frac{\partial E_z}{\partial \theta} = \frac{\partial B_r}{\partial t} \quad (4-2)$$

$$\therefore E_z = \int \left[-r \frac{\partial B_r}{\partial t} \right] d\theta \quad (4-3)$$

In steady state condition $\frac{\partial \Omega_f(r)}{\partial t} = 0$ therefore Equation (4-3) becomes

$$E_z = (u - r\Omega) B_r \quad (4-4)$$

Where $u = r\Omega_f$ is the azimuthal fluid velocity. The Lorentz forces induced in the fluid which is in the direction of fluid flow can be expressed by:

$$F_\theta = -J_z B_r = \sigma (r\Omega - u) B_m^2 \sin^2(p(\Omega - \Omega_f(r))t - p\theta) \quad (4-5)$$

The fluid flow is laminar, and due to the symmetry of the system, It is considered that fluid velocity varies only in radial direction. Therefore the azimuthal velocity variation u and pressure P according to azimuthal coordinate θ are zero in the Navier-stokes equation [33]. The governing equation for MHD in steady state is reduced to Equation (4-6), where μ is the dynamic viscosity of the fluid.

$$\frac{\partial^2 u}{\partial r^2} + \frac{1}{r} \frac{\partial u}{\partial r} - \frac{u}{r^2} = \frac{F_\theta}{\mu} \quad (4-6)$$

By considering the mean value of the Lorentz forces with $\lambda = \sqrt{0.5\sigma\mu^{-1}B_m^2}$ Equation (4-6) becomes

$$\frac{\partial^2 u}{\partial r^2} + \frac{1}{r} \frac{\partial u}{\partial r} - \left(\frac{1}{r^2} + \lambda^2 \right) u = -\lambda^2 r \Omega \quad (4-7)$$

The general solution of Equation (4-7) is given in Equation (4-8) where $I_1(\cdot)$ is the first order modified Bessel function of the first kind and $K_1(\cdot)$ is second kind.

$$u = AI_1(\lambda r) + BK_1(\lambda r) + r\Omega \quad (4-8)$$

The constant A and B can be determined by using boundary condition as given in (4-9).

$$u = \begin{cases} R_i \Omega & \text{when } r = R_i \\ 0 & \text{when } r = R_o \end{cases} \quad (4-9)$$

$$A = -\frac{R_o \Omega K_1(\lambda R_i)}{K_1(\lambda R_i)I_1(\lambda R_o) - K_1(\lambda R_o)I_1(\lambda R_i)} \quad (4-10)$$

$$B = \frac{I_1(\lambda R_i)R_o \Omega}{K_1(\lambda R_i)I_1(\lambda R_o) - K_1(\lambda R_o)I_1(\lambda R_i)} \quad (4-11)$$

The fluid velocity of the homogeneous solution (u_0) in the case when no magnetic field is applied can be derived by solving Equation (4-6) under boundary conditions (4-9) with $\eta = R_i/R_o$.

$$u_0 = \frac{\Omega \left(\eta^2 r - \frac{R_i^2}{r} \right)}{(\eta^2 - 1)} \quad (4-12)$$

Fig. 4-2 shows the difference in velocity of the fluid when magnetic flux density is applied and when no magnetic flux density in the present in the stator-rotor gap in the radial direction calculated via Equation (4-8) and (4-12) respectively. The velocity variation observed in the fluid is due to the electromechanical power transmitted in the fluid due to the Lorentz forces generated, as seen in Fig. 4-3.

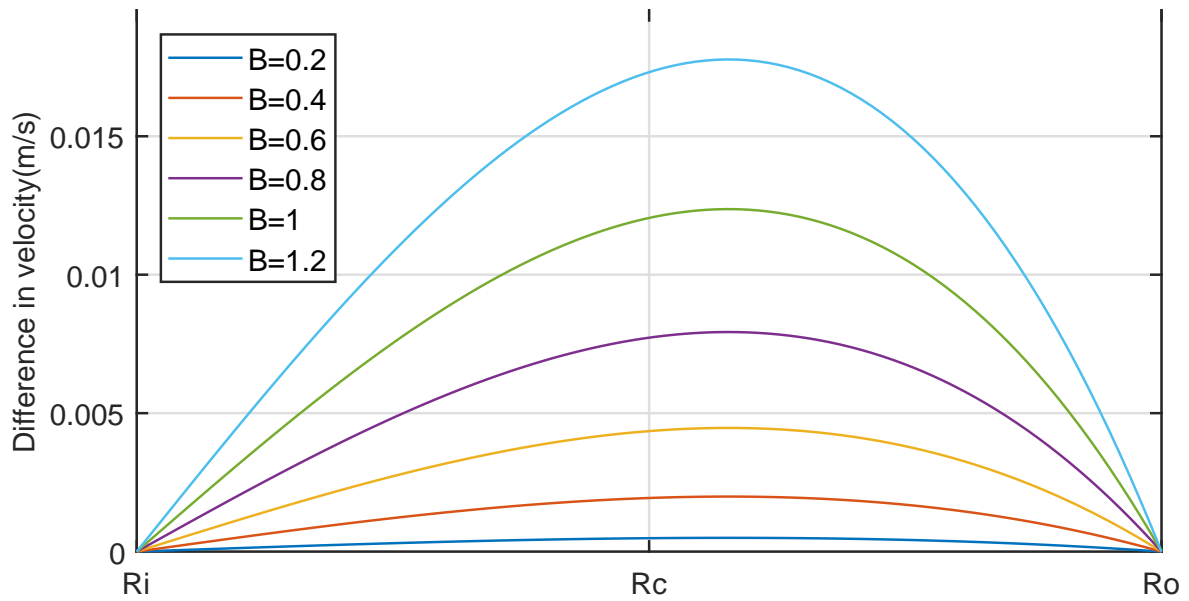


Figure 4-2: Fluid velocity variation for different values of the magnetic flux density radially

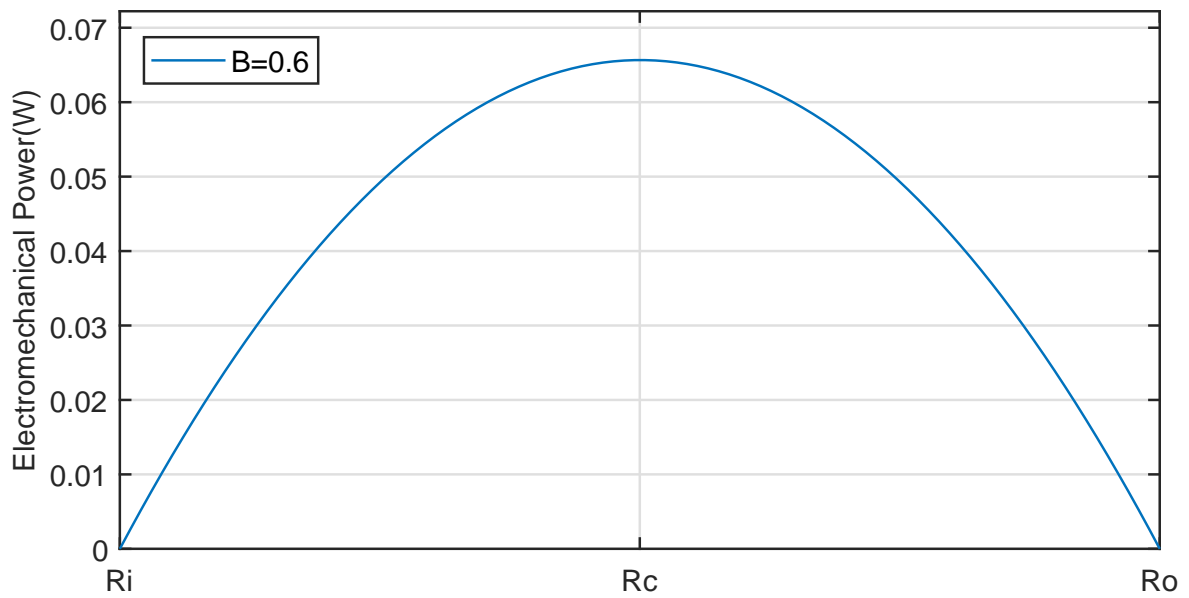


Figure 4-3: Electromechanical power transmitted vs stator rotor gap in radial direction evaluated by using Equation 4-14

Fig. 4-4 shows the induced current density in the seawater at different magnetic flux density. The water at rotor surface is rotating at the same speed as the rotor hence the induced current density in seawater at rotor surface is zero while the water at stator surface is stationary hence the highest current density can be seen there. It can also be observed that the current density is directly proportional to magnetic flux density. The induced current density is also directly proportional to the rotor velocity which shown in Appendix C.

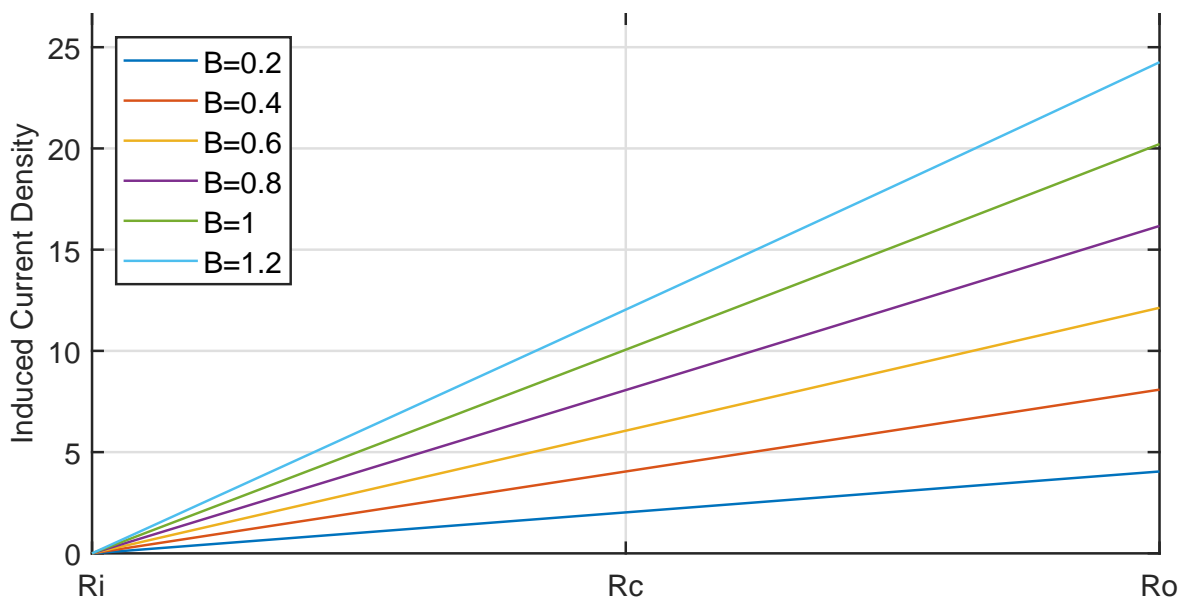


Figure 4-4: Eddy currents in the stator-rotor gap for different values of the magnetic flux densities radially

Fig. 4-5 shows the magnetic flux density under two conditions. First, the seawater is assumed to be stationary initially while the velocity in seawater is imparted due to rotor motion. The velocity profile of seawater in stator rotor gap in the radial direction is shown in Fig. 4-6. The magnetic flux density in the gap is also assumed to be constant. Second, The sea water in stator-rotor gap is considered to be a sleeve, and the whole water is rotating at the same velocity as that of rotor surface. In this case, the magnetic flux density considered is with harmonics as well.

It can be observed that induced current density at the rotor surface (R_i) is not zero for case II as is in case I. This is due to the harmonics present in the magnetic flux density. The Induced current density at the stator surface (R_o) is lower in case II than that in case I, because the sea water is stationary in case I while that in case II is rotating at the same velocity as rotor surface. It can also be observed that the induced current density under harmonic condition changes exponentially with respect to the magnetic flux density while under constant magnetic flux density it changes linearly. It can be said that induced current density in the sea water considering the harmonic magnetic flux density for the laminar flow will be higher than that shown in Fig. 4-5.

4-4 MHD Losses

Joule losses present in the water are due to induced current density. The electromechanical power is transmitted in the water is due to the Lorentz force and friction is present due to the fluid viscosity

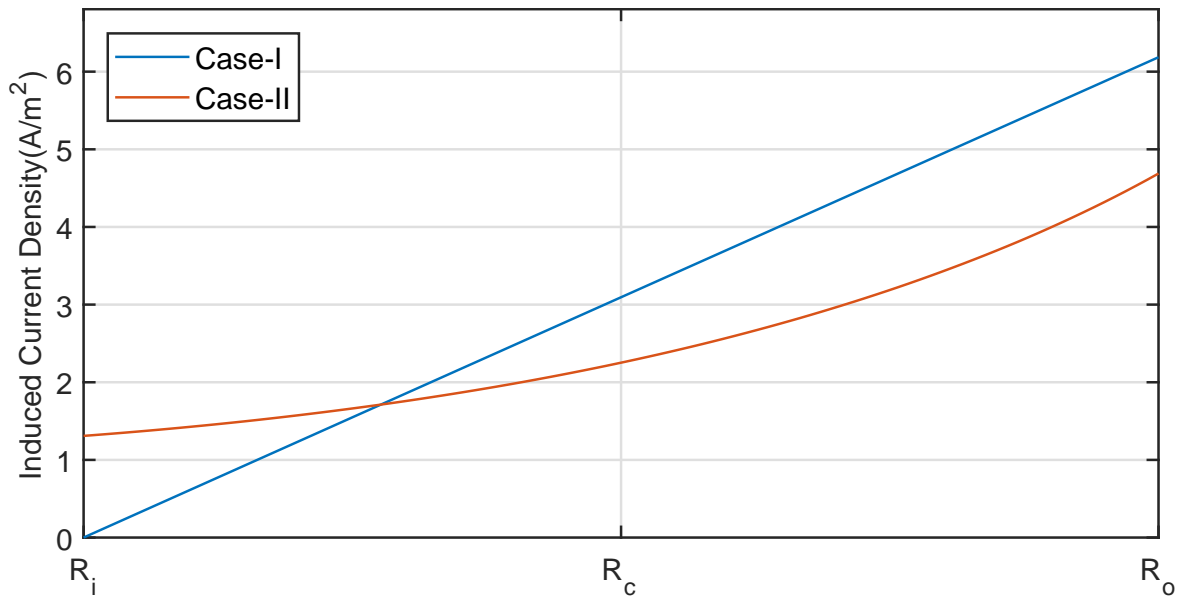


Figure 4-5: Eddy currents in the stator-rotor gap for stationary and rotating seawater

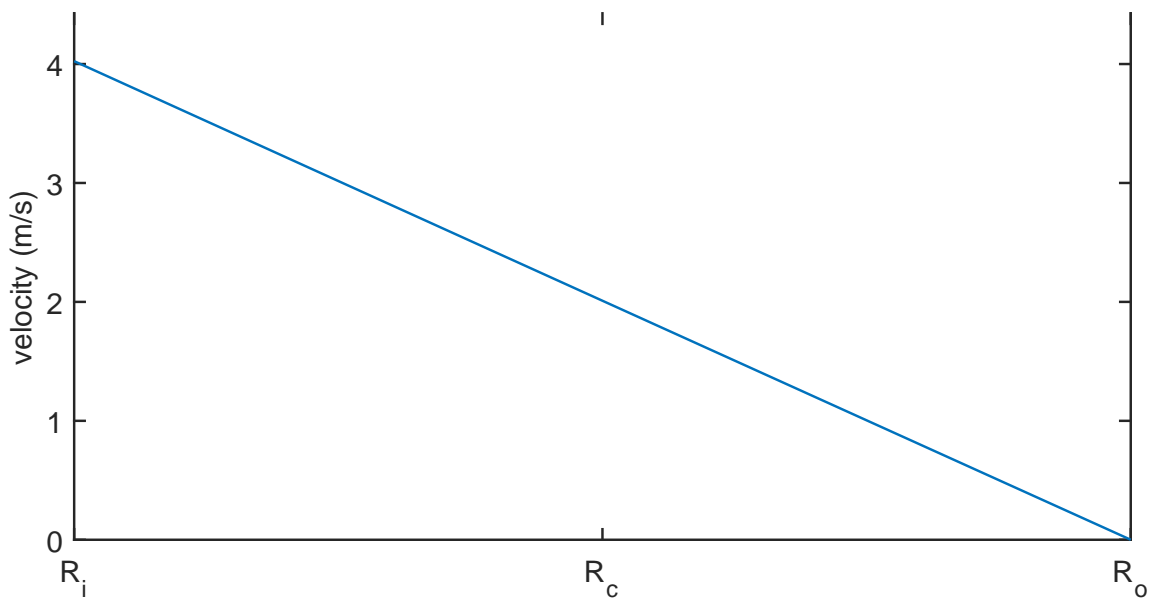


Figure 4-6: Seawater velocity under no load condition

which creates skin friction shear stress on the rotor surface [33]. The friction at the stator surface will be zero as the sea water is stationary. The Joule losses can be evaluated by Equation 4.17, where L is the axial length of the stator rotor gap.

$$P_j = -\sigma B_m^2 \pi L \int_{R_i}^{R_o} (u - r\Omega)^2 r dr \quad (4-13)$$

The electromechanical power can be calculated by considering only the mean value of the Lorentz forces.

$$P_{em} = -\sigma B_m^2 \pi L \int_{R_i}^{R_o} (u - r\Omega) u r dr \quad (4-14)$$

The friction on the rotor surface is proportional to the derivative of the velocity with respect to the radial direction [33]. By replacing u with $(\Delta u = u - u_0)$ in Equation (4-15), we can obtain the friction power loss in on the rotor surface due to the magnetic field. $I_0(\cdot)$ and $K_0(\cdot)$ in Equation (4-16) are the zero order modified Bessel function of first kind and second kind respectively.

$$P_\mu = \int_{RS} \mu u(R_i) \left(\frac{\partial u}{\partial r} - \frac{u}{r} \right)_{r=R_i} ds \quad (4-15)$$

$$\Delta P_\mu = 2\pi\mu LR_i^2 \Omega \left[A \left(I_0(\lambda R_i) - \frac{I_1(\lambda R_i)}{\lambda R_i} \right) \lambda + B \left(-K_0(\lambda R_i) - \frac{K_1(\lambda R_i)}{\lambda R_i} \right) \lambda + \Omega - \frac{AI_1(\lambda R_i) + BK_1(\lambda R_i) + R_i \Omega}{R_i} \right] \quad (4-16)$$

Table 4-2: Loss associated With MHD

Sr No	Description	Loss (W)
1	Joule Loss	0.0833
2	Friction Loss	0.0437
3	Electromechanical Power	0.0433
4	MFD free friction loss	15.23

The friction loss and electromechanical power are equal as shown in Table 4-2 because the friction between the fluid particles is neglected. As seen in Fig 4-2 the maximum variation in fluid velocity does not occur at the stator surface, but it is closer to stator surface than rotor surface which is coherent with the electromechanical power in the gap.

4-5 Conclusion

The Joule losses in the seawater in the stator rotor gap will be higher under harmonic magnetic flux density. As there is compensation between the P_{em} and ΔP_μ , the total MHD loss in the system is nearly equal to the Joule losses (P_j) and MFD free friction loss which is the predominant one. The Joule losses are less than 0.005% of the iron loss under constant magnetic flux density in stator rotor gap, even though the Joule losses under the harmonic magnetic flux they will not be a significant amount. Hence MHD losses can be neglected during the designing process.

Chapter 5

Thermal Model

5-1 Introduction

Heat transfer occurs whenever there exist temperatures difference in a medium or between media. There are three modes of heat transfer. Firstly, when a temperature gradient exists in a stationary medium; it is termed as conduction. Secondly, convection occurs when there exists temperature difference between a surface and a moving fluid. The third mode is termed thermal radiation, as all surfaces of finite temperature emit energy in the form of electromagnetic waves. The convection heat transfer can be further classified according to the nature of the flow. Forced convection happens when the flow is caused by external means such as fan or pump. While the free or natural convection occurs when the flow is induced by buoyancy forces, which are due to density caused by temperature variations in the fluid [46].

This chapter develops a lumped circuit model for tidal generators to evaluate the temperature distribution inside the machine based on the losses in the various parts of the generator. The aim of building the thermal model is to assess which retaining material is most suitable for tidal generators.

5-2 Thermal Model

For thermal analysis, the machine can be divided geometrically into a number of lumped components, each component having a bulk thermal storage and heat generation and interconnections to adjacent components through a linear mesh of thermal impedances. The lumped parameters are derived from dimensional information, the thermal properties of the material used in the design, and heat transfer coefficients [8].

5-2-1 Thermal Conduction

The thermal resistance $R_{th} = L / (A\lambda)$ describes the conductive heat transfer in one direction, where A is the cross-sectional area, λ is the thermal conductivity, and L is the length of the body in the

heat flow direction. A base component of all the machine parts having cylindrical form is a general cylindrical component. The general cylindrical component is described in the following section.

General Cylindrical Components

The solid components of the machine are based on the general cylindrical component shown in Fig. 5-1a. To obtain simple, but physically significant, expressions for the network of thermal resistances that describe the heat conduction across the general component, the following assumptions are made

1. The heat flow in both radial and axial direction are defined by a single mean temperature.
2. The heat flow in the radial and axial directions are independent.
3. Circumferential heat flow in the stator and rotor yoke is zero.
4. The thermal capacity and heat generation are uniformly distributed.

Based on these assumptions the solution of the heat conduction equations in each of the axial and radial directions produces the two separate three terminal network as shown in Fig. 5-1b. In each network, two terminals represent the appropriate surface temperature of the component, whereas the third represents the mean temperature θ_m of the component at which any internal heat generation u or thermal storage c is introduced. The central node of each network would give the mean temperature of the component if there were no internal heat generation or storage [8]. The values of the thermal

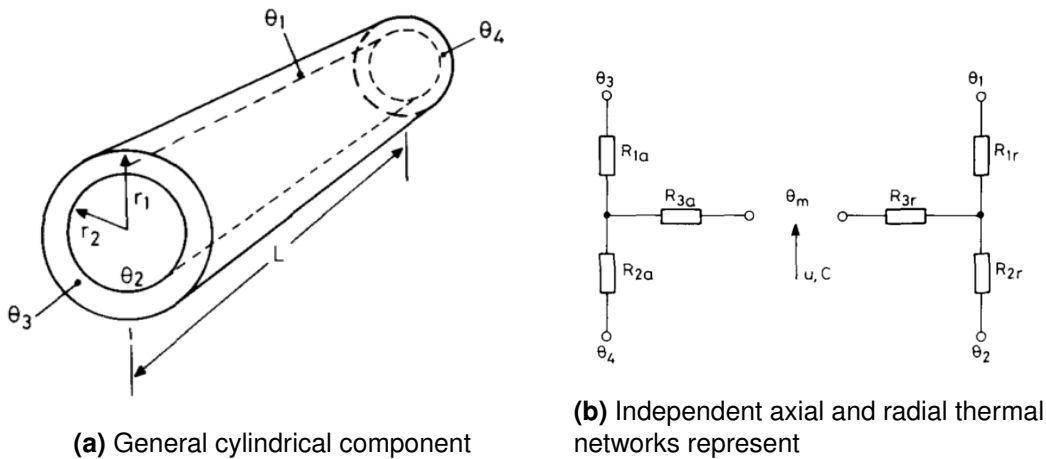


Figure 5-1: Basic Thermal Model [8]

resistances in each network come directly from the independent solutions of the heat conduction equations in the axial and radial directions. Where k_a is thermal conductivity of the material in axial direction and k_r is thermal conductivity of the material in radial direction. The negative resistance represent that heat can not flow in reverse direction [8].

$$R_{1a} = \frac{L}{2\pi k_a (r_1^2 - r_2^2)} \quad (5-1)$$

$$R_{2a} = \frac{L}{2\pi k_a(r_1^2 - r_2^2)} \quad (5-2)$$

$$R_{3a} = \frac{-L}{6\pi k_a(r_1^2 - r_2^2)} \quad (5-3)$$

$$R_{1r} = \frac{1}{4\pi k_r L} \left[1 - \frac{2r_2^2 \ln\left(\frac{r_1}{r_2}\right)}{(r_1^2 - r_2^2)} \right] \quad (5-4)$$

$$R_{2r} = \frac{1}{4\pi k_r L} \left[\frac{2r_1^2 \ln\left(\frac{r_1}{r_2}\right)}{(r_1^2 - r_2^2)} - 1 \right] \quad (5-5)$$

$$R_{3r} = \frac{-1}{8\pi(r_1^2 - r_2^2)k_r L} \left[(r_1^2 + r_2^2) - \frac{4r_1^2 r_2^2 \ln\left(\frac{r_1}{r_2}\right)}{(r_1^2 - r_2^2)} \right] \quad (5-6)$$

The two one-dimensional networks are combined simply by connecting the points of mean temperature together. If it is assumed that the temperatures in the cylinder are symmetrical about a central radial plane so that the face temperatures θ_3 , and θ_4 , are equal, it is only necessary to model half the cylinder with correspondingly only half the heat generation and thermal capacitance [8]. The thermal

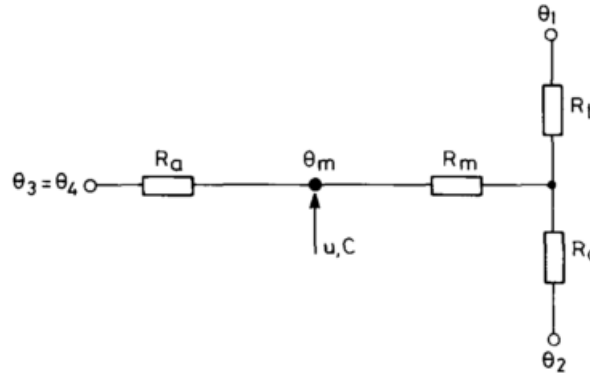


Figure 5-2: Combined thermal network for symmetric component

network is then reduced to the form shown in Fig. 5-2, which consists of two internal nodes and four thermal resistances, R_a, R_b, R_c and R_m given by

$$R_a = \frac{L}{6\pi k_a(r_1^2 - r_2^2)} \quad (5-7)$$

$$R_b = \frac{1}{2\pi k_r L} \left[1 - \frac{2r_2^2 \ln\left(\frac{r_1}{r_2}\right)}{(r_1^2 - r_2^2)} \right] \quad (5-8)$$

$$R_{bc} = \frac{1}{2\pi k_r L} \left[\frac{2r_1^2 \ln\left(\frac{r_1}{r_2}\right)}{(r_1^2 - r_2^2)} - 1 \right] \quad (5-9)$$

$$R_m = \frac{-1}{4\pi(r_1^2 - r_2^2)k_r L} \left[(r_1^2 + r_2^2) - \frac{4r_1^2 r_2^2 \ln\left(\frac{r_1}{r_2}\right)}{(r_1^2 - r_2^2)} \right] \quad (5-10)$$

The resistances R_b and R_c represent the thermal conduction resistance in the radial direction, while the resistance R_a represent the thermal conduction resistance in the axial direction. R_m takes into account the heat that is not transferred in the previous resistance. Where r_1 and r_2 are the inner and outer radius of the considered cylinder, k_a is the conduction coefficients and L is the cylindrical length.

Equations (5-11) & (5-12) are the thermal resistances computed by well-known equations of heat transfer in hollow cylinders [46][43]. Fig. 5-3 shows the percentage error in thermal resistances calculated for a unitary value of the thermal conduction coefficient via Equation (5-11) & (5-12) and Equations (5-8) & (5-9). Taking into account that the ratio r_2/r_1 is less than 1.1, the percentage error introduced by the simplified equations is less than 1%. This error is much lower than the uncertainty on the convection resistance computation [43]. Hence for further calculations, the simplified formula will be used.

$$R_1 = \frac{1}{2\pi k_r L} \ln\left(\frac{r_m}{r_1}\right) \quad (5-11)$$

$$R_2 = \frac{1}{2\pi k_r L} \ln\left(\frac{r_2}{r_m}\right) \quad (5-12)$$

Where

$$r_m = \frac{r_1 + r_2}{2} \quad (5-13)$$

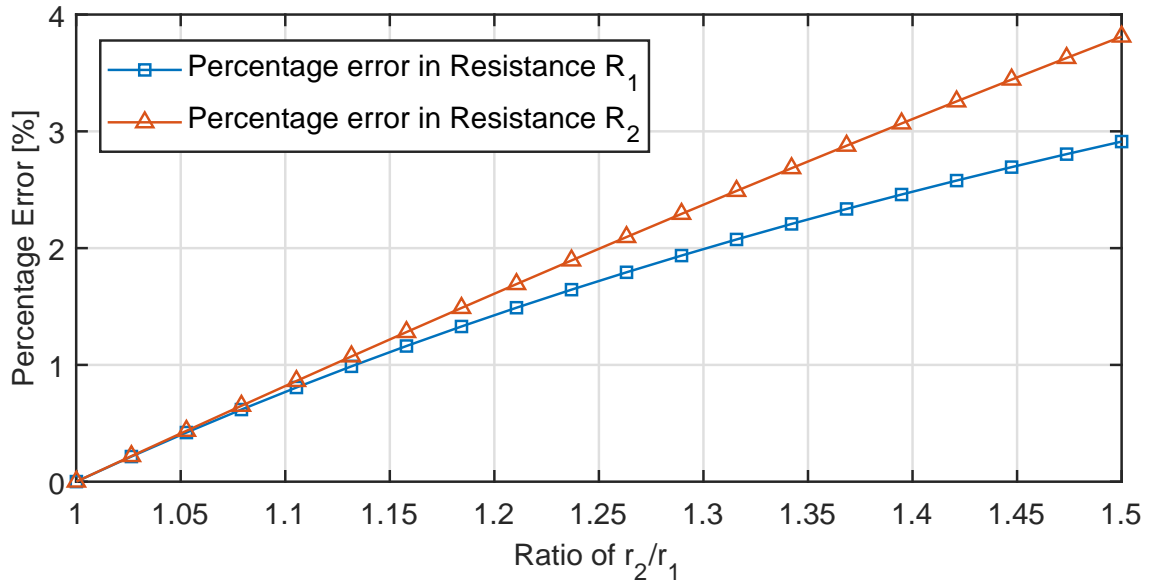


Figure 5-3: Percentage of error in thermal resistance at different ratio of r_2/r_1

5-2-2 Thermal Convection

The convection of heat between the solid surfaces and the fluid is modeled using a single thermal resistance $R_{convection}$ defined as:

$$R_{convection} = \frac{1}{hA} \quad (5-14)$$

Where h is the convection coefficient, and A is the surface area. The convection thermal resistances for tidal generators are listed below.

1. Thermal convection from generator frame to the seawater.
2. Thermal convection from the stator retaining sleeve to stator-rotor gap seawater.
3. Thermal convection from the rotor retaining sleeve to stator-rotor gap seawater.
4. Thermal convection from surface of the end winding to the seawater in end cap.
5. Thermal convection from surface of the rotor yoke, stator yoke and permanent magnets to the seawater in end cap.

Detailed description how to calculate the natural and forced convection coefficients for general geometry is given below.

5-2-3 Heat Transfer Coefficient

The heat transfer coefficient is $h = NuK/\delta$, where Nu is the Nusselt number, K is the thermal conductivity of the medium and δ is the characteristic length of the geometry. The Nusselt number for a cylinder can be written as follows [31] [44].

$$Nu_{cylinder} = \left(0.6 + 0.387Ra_D^{0.166} (1 + 0.721Pr^{-0.5625})^{-0.296}\right)^2 \quad (5-15)$$

and for vertical plates, it can be written as follows:

$$Nu_{plates} = \left(0.825 + 0.387Ra_D^{0.166} (1 + 0.671Pr^{-0.5625})^{-0.296}\right)^2 \quad (5-16)$$

Assuming forced convection for the cylindrical surface around the frame, it is expressed as follows:

$$Nu_{cylinder} = 0.3 + 0.62Re_D^{0.5} Pr^{0.333} (1 + 0.000392Re_D^{0.625})^{0.8} (1 + 0.543Pr^{-0.667})^{-0.25} \quad (5-17)$$

and for vertical plates, it is expressed as follows:

$$\begin{cases} Nu_{plates} = 0.664Re_D^{0.5} Pr^{0.333} & Re_L < 500000 \\ Nu_{plates} = (0.037Re_D^{0.8} - 871) Pr^{0.333} & Re_L \geq 500000 \end{cases} \quad (5-18)$$

Where Ra is Rayleigh number, Re is Reynolds number and Pr is Prandtl number.

$$Pr = \frac{c_p \mu}{k_f} \quad (5-19)$$

$$Re_{D,plate} = \frac{VD}{\nu} \quad (5-20)$$

$$Re_{D,cylinder} = \frac{\omega D^2}{2\nu} \quad (5-21)$$

$$Ra_D = \frac{g\beta (T_s - T_\infty) \delta^3}{\nu^2} Pr \quad (5-22)$$

Where c_p is the specific heat, k_f is thermal conductivity, ρ is fluid density, μ fluid viscosity, V is the fluid velocity in m/s, ω is the angular velocity of rotor, D is outer diameter of cylinder, g is gravitational acceleration, T_s is temperature of surface, T_∞ is temperature of fluid/ambient $\beta = 1/(T_s + T_\infty)/2$ is coefficient of volume expansion, ν is kinematic viscosity of the fluid, and δ is the characteristic length of the geometry i.e. $\delta = A_s/P_s$, A_s is the area of the surface and P_s is the periphery of the surface.

5-2-4 Thermal Radiation

Thermal Radiation is the energy emitted by the matter that is at nonzero temperature. The radiation heat removal rate depends on the temperature difference and the position between the heat-exchanging surfaces. The radiation heat transfer coefficient is [45][46]:

$$h_r = \varepsilon \sigma (T_s + T_{sur}) (T_s^2 + T_{sur}^2) \quad (5-23)$$

where ε is a radioactive property of the surface i.e. a measure of how efficiently a surface emits energy relative to blackbody with a value in the range $0 \leq \varepsilon \leq 1$ and $\sigma = 5.67 \times 10^{-8} \text{W/m}^2/\text{K}^4$ is the Stefan-Boltzmann constant.

Due to the low-temperature gradient inside the machine, i.e. between the end windings & the frame and the stator winding & the stator teeth the thermal radiation inside electrical machines is not as significant as a heat transfer from the thermal convection and thermal conduction [30]. Therefore only the thermal resistances between the frame and the ambient, the end winding and the end cap, and the stator retaining sleeve and the stator rotor gap are considered.

5-3 Models of Thermally Conductive Parts

5-3-1 Thermal Model of Stator and Rotor Yoke

For modeling, the stator and rotor yoke they can be considered as hollow cylinders made up of the numerous iron laminations, so the heat transfer in the radial direction will be much higher than that in the axial direction. The parameters of the yoke can be calculated based on Equation (5-24) to (5-27) where $k_{iron,r}$ is the thermal conductivity of iron in radial direction and $k_{iron,a}$ is the thermal conductivity of iron in the axial direction [43] [8]. The Parameters of the stator yoke can be given as follows.

$$R_{th5} = \frac{1}{2\pi k_{iron,r} L_s} \ln\left(\frac{r_1}{r_m}\right), \quad (5-24)$$

$$R_{th6} = \frac{1}{2\pi k_{iron,r} L_s} \ln\left(\frac{r_m}{r_2}\right), \quad (5-25)$$

$$R_{th4} = \frac{-1}{4\pi(r_1^2 - r_2^2)k_{iron,r}L_s} \left[(r_1^2 + r_2^2) - \frac{4r_1^2 r_2^2 \ln\left(\frac{r_1}{r_2}\right)}{(r_1^2 - r_2^2)} \right], \quad (5-26)$$

$$R_{th3} = \frac{L}{6\pi k_{iron,a}(r_1^2 - r_2^2)}. \quad (5-27)$$

Where r_1 is the outer radius of the yoke, r_2 is the inner radius of the yoke, and $r_m = (r_1 + r_2)/2$.

5-3-2 Thermal Model of Stator Teeth

The stator teeth can be modeled by considering a collection of segments connected thermally in parallel. The arc length of the cylinder is considered to equal to the cross-sectional area of the teeth. Resistance R_{th8} is added to take into account the circumferential heat flow from teeth to winding. The thermal model of the stator teeth is given in Fig. 5-4. The thermal parameters are given as below:

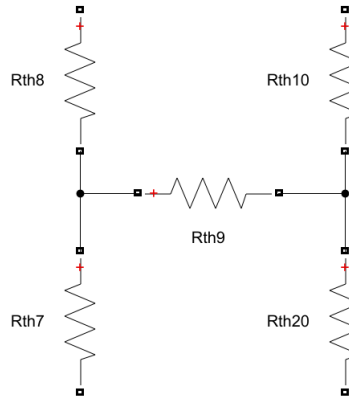


Figure 5-4: Thermal Model of stator teeth

$$R_{th10} = \frac{\phi_p}{2\pi k_{iron,r} \phi_e L_s} \ln\left(\frac{r_1}{r_m}\right), \quad (5-28)$$

$$R_{th11} = \frac{\phi_p}{2\pi k_{iron,r} \phi_e L_s} \ln\left(\frac{r_m}{r_2}\right), \quad (5-29)$$

$$R_{th9} = \frac{-\phi_p}{4\pi(r_1^2 - r_2^2)k_{iron,r} \phi_e L_s} \left[(r_1^2 + r_2^2) - \frac{4r_1^2 r_2^2 \ln\left(\frac{r_1}{r_2}\right)}{(r_1^2 - r_2^2)} \right], \quad (5-30)$$

$$R_{th7} = \frac{L\phi_p}{6\phi_e \pi k_{iron,a} (r_1^2 - r_2^2)}, \quad (5-31)$$

$$R_{th8} = \frac{\pi \phi_e (r_1^2 - r_2^2)}{L_s \phi_p \pi k_{iron,r} (r_1 - r_2)^2 z^2}. \quad (5-32)$$

Where r_1 is the outer radius of the stator teeth, r_2 is the inner radius of the stator teeth, and $r_m = (r_1 + r_2)/2$. ϕ_p is tooth width, ϕ_e is slot pitch, and z is number of slots.

5-3-3 Thermal Model of Stator Winding

For modeling stator winding it considered as solid cylindrical rod consisting of arrays of conductors and insulation. It is assumed that the copper transfers heat axially along the slot. It is assumed that the winding only conducts heat in the axial direction only. While in the radial direction the winding has a uniform conductivity which is proportional to the conductivities of the varnish and the enamel. Hence the heat conductivity of copper in the radial direction is not considered. In [47], It is suggested that the rod equivalent conductivity factor F depends only on the slot fill factor. Measurement conducted

by [47] suggest that the F values varies between 2 – 4 for a slot fill factor of 0.4 – 0.6. Hence for the present machine, the $F = 4$ is considered. The thermal parameters for stator slot winding as given as below:

$$R_{th12} = \frac{2d_i}{\pi k_i L_s r z} + \frac{1}{2\pi k_v L_s F z}, \quad (5-33)$$

$$R_{th13} = \frac{L}{6k_c A_c z}, \quad (5-34)$$

$$R_{th14} = \frac{4d_i}{\pi k_i L_s r z} + \frac{1}{\pi k_v L_s F z}, \quad (5-35)$$

$$R_{th15} = \frac{1}{\pi k_v L_s F z}. \quad (5-36)$$

where r is the equivalent winding radius, $d_i = 0.5\text{mm}$ is the insulation thickness, k_c in thermal conductivity of copper at 27°C , k_i is the thermal conductivity of slot liner, k_v is the thermal conductivity of varnish at 27°C , and F is the radial conductivity factor.

5-3-4 Thermal Model of the Retaining Sleeves

The retaining sleeve can be modeled based on the general cylindrical component. The retaining sleeve is single sheet material. Hence the thermal conductivity in both the axial and the radial direction are considered as similar. For thermal parameters refer Equations (5-11), (5-12), (5-7) and (5-10).

5-3-5 Thermal Model of Airgap

The convection heat transfer in stator-rotor gap due to the rotation has been modeled as turbulent fluid flow between rotating cylinders. In this case, the axial heat transfer in stator-rotor gap is ignored compared with the radial heat transfer. Based on the turbulent flow of the fluid in the stator-rotor gap, the fluid is considered to have the velocity equal to the outer surface of the retaining sleeve. Therefore Nusselt number for the convection heat transfer between fluid and stator will be as follows [43], [48], [31], [46]:

$$N_{uD} = 0.0296 Re_D^{4/5} Pr^{1/3} \quad (5-37)$$

As the velocities of the rotor and seawater are almost the same, the heat transfer between them is modeled by conduction. Thus, the thermal resistance between the seawater and rotor retaining sleeve can be expressed as follows [31], [46]:

$$R_{th44} = \frac{1}{2\pi k_{seawater} L_s} \ln\left(\frac{r_2}{r_1}\right) \quad (5-38)$$

Where r_2 and r_1 is the outer and inner stator-rotor gap radius respectively.

5-3-6 Thermal Model of End Winding

The model parameters for end windings are calculated as follows. The thermal conductive resistance between end winding and slot winding is [48]

$$R_{th19} = \frac{l_e/2}{2k_{cu} N_c A_{cu}} \quad (5-39)$$

The thermal resistance between middle end windings (i.e., middle equivalent cylinder) and exterior surface of end winding (i.e., surface of equivalent cylinder) is [48]

$$R_{th20} = \frac{1}{2\pi F k_v h_t} \ln\left(\frac{r_{e2}}{r_m}\right) \quad (5-40)$$

where, $r_m = (r_{e1} + r_{e2})/2$, and r_{e1} and r_{e2} are interior and exterior radii of the equivalent cylinder of the end winding. The specifications such as F, k_v, k_{cu}, A_{cu} are calculated in the same way as that of the slot winding. The average end winding length is

$$l_e = \pi \frac{r_{e1} + r_{e2}}{2} \quad (5-41)$$

where $r_{e1} = W_t/2, r_{e2} = (W_t + 2N_{layer}d_{Cu} + 2d_i)/2$, and h_t and W_t are respectively the height and width of a tooth and N_{layer} is the number of winding layers.

5-3-7 Thermal Model of Permanent Magnet

Magnets are assumed to produce a cylinder, including two parts in a pole pitch, namely, magnet and air. Therefore, the thermal model of magnets has two parallel branches as shown in Fig. 5-5. The model parameters are given as follows [48]

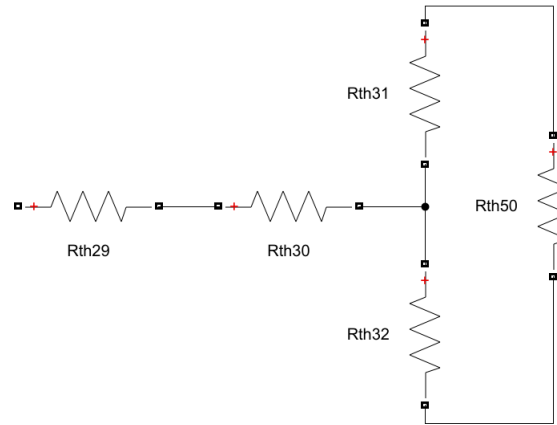


Figure 5-5: Thermal Model of Permanent Magnet region

$$R_{th31} = \frac{\pi}{2\tau_e} \frac{1}{2\pi k_{pm} \tau_p L_m} \ln\left(\frac{r_{ipm}}{r_{rpm}}\right), \quad (5-42)$$

$$R_{th32} = \frac{\pi}{2\tau_e} \frac{1}{2\pi k_{pm} \tau_p L_m} \ln\left(\frac{r_{opm}}{r_{rpm}}\right), \quad (5-43)$$

$$R_{th30} = \frac{-\tau_p}{4\pi(r_{ipm}^2 - r_{opm}^2)k_{pm}\tau_e L_s} \left[(r_{ipm}^2 + r_{opm}^2) - \frac{4r_{ipm}^2 r_{opm}^2 \ln\left(\frac{r_{ipm}}{r_{opm}}\right)}{(r_{ipm}^2 - r_{opm}^2)} \right], \quad (5-44)$$

$$R_{th29} = \frac{L\tau_e}{6\tau_p \pi k_{pm} (r_{ipm}^2 - r_{opm}^2)}, \quad (5-45)$$

$$R_{th50} = \frac{\pi}{\pi - 2\alpha} \frac{1}{2\pi k_{air} L_m} \ln\left(\frac{r_{opm}}{r_{ipm}}\right). \quad (5-46)$$

Where L_m is the length in the axial direction, r_{opm} is the outer radius of the permanent magnet r_{ipm} is the inner radius of the permanent magnet, $r_{pm} = (r_{ipm} + r_{opm})/2$ is the mean radius of the magnet, k_{pm} is the conductive heat transfer of the magnet, τ_e is the magnet width and τ_p is the pole pitch.

5-3-8 Thermal Model of End Cap

In endcap region, materials are in contact with circulating seawater, whose temperature is assumed to be uniform, a single film coefficient is used to model the heat transfer to and from all the surfaces in contact with circulating endcap seawater. Even though not all the surface materials are same, we have considered single film coefficient as complex analysis is required to evaluate each case, and this can not be justified, considering the accuracy of which they can be obtained [8]. Stator and rotor surfaces can be modeled as vertical plate in contact with seawater while the end windings can be considered as a cylindrical surface. For heat transfer coefficient calculation refer section 5-2-3.

5-3-9 Thermal Model of The Shaft

The shaft is modeled as a cylindrical rod with no internal heat generation. The heat conduction in the axial direction is modeled in three sections, one under the rotor yoke, second under the bearing and third that acts as a thermal connection between the mean temperature of the first two. It is assumed that there is good thermal contact between the shaft and the frame. The Thermal Parameters of the shaft are given below.

$$R_{shaft1} = \frac{1}{2\pi k_s L_s} + \frac{l_m}{2\pi k_s r} \quad (5-47)$$

Where, K_s is the thermal conductivity of shaft, l_m is distance of the bearing center to rotor mean, l_b is bearing housing width and r is the shaft radius.

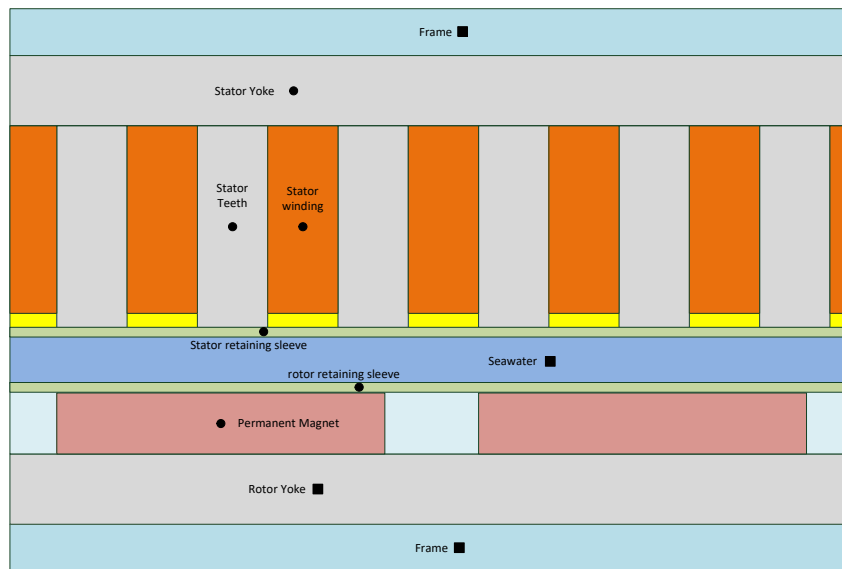
5-4 Results

The thermal conductance considered for various materials in the model are given in Table 5-1 [46] [48]. It is considered that the machine is submerged in seawater hence the ambient temperature is considered as 16 degrees. For calculation of the heat transfer coefficient from the frame of the machine, the velocity of water flow is considered as 2m/s. Fig. 5-6 shows the nodes considered in the thermal model. The point represented by the circle is the heat generation source. The complete thermal model and description of the thermal resistances are mentioned in Appendix D.

Table 5-2 shows, the temperature in the machine when losses in only the rotor retaining sleeve of configuration-1 used while the Table 5-3 shows the temperatures when configuration-2 is used. It can be observed that temperatures in Table 5-3 are higher than that in Table 5-2, this because of the losses in the sleeve for configuration-2 is very high than that in configuration-1 due to the presence of the copper sleeve. The temperature in the machine is remaining same when different retaining sleeve materials are used because the eddy current losses in the retaining sleeves are very small as compare to the iron and copper loss. It can also be observed that the temperature in the titanium sleeve is

Table 5-1: Thermal conductance of different materials

Sr No	Symbol	Thermal Conductivity	Value(W/m/K)
1	$k_{iron,r}$	Stator iron radial direction	30
2	$k_{iron,a}$	Stator iron axial direction	0.6
3	k_i	Slot Liner	0.15
4	k_v	Varnish	0.18
5	k_c	Copper	401
6	$k_{seawater}$	Seawater	0.6
7	k_{air}	air	0.5
8	k_{pm}	Permanent Magnet	30
9	$k_{sleeve,s}$	Stator retaining sleeve, (steel)	16.2
10	$k_{sleeve,r}$	Rotor retaining sleeve, (steel)	16.2
11	k_s	Shaft	50

**Figure 5-6:** The node placement for the thermal model**Table 5-2:** Temperature in different part of the machine with only rotor retaining sleeve

Sr. No	Retaining Sleeve Material	Stator Yoke	Stator Teeth	Stator Winding	End Winding	Stator retaining sleeve	Rotor retaining sleeve	Permanent Magnet	Rotor yoke
1	Inconel	42.73	44.66	52.69	51.60	47.08	38.11	37.79	37.34
2	Steel	42.75	44.68	52.71	51.62	47.09	38.13	37.82	37.36
3	Hastelloy	42.73	44.66	52.69	51.60	47.08	38.12	37.79	37.34
4	Titanium	42.73	44.66	52.70	51.60	47.10	38.14	37.78	37.33

Table 5-3: Temperature in different part of the machine with copper sleeve and rotor retaining sleeve

Sr. No	Retaining Sleeve Material	Stator yoke	Stator teeth	Stator winding	End winding	Stator retaining sleeve	Copper sleeve	Rotor retaining sleeve	Permanent magnet	Rotor yoke
1	Inconel	44.05	46.04	54.06	52.95	48.67	39.64	39.56	39.18	38.65
2	Steel	44.06	46.05	54.07	52.96	48.68	39.62	38.56	39.21	38.67
3	Hastelloy	44.05	46.04	54.06	52.95	48.68	39.66	39.57	39.18	38.64
4	Titanium	44.05	46.50	54.06	52.95	48.70	39.73	39.60	39.17	38.64

higher than that in the steel sleeve even though the titanium sleeve have lower losses, this is because the thermal conductivity of titanium is less than half of that steel.

Table 5-4 shows, the temperature in the machine when losses in both the stator and rotor retaining sleeves are considered. The temperature in the machine has increased substantially as compared to Table 5-2 and 5-3 because the losses in the stator sleeve are higher than iron and copper losses. Here we observe the temperature in the machine with titanium sleeve is lowest even though it has the lowest thermal conductivity among the materials selected, because the losses in the titanium sleeve are the lowest and the difference in the losses are also substantial.

Table 5-4: Temperature in different part of the machine with stator and rotor retaining sleeve

Sr. No	Retaining sleeve material	Stator Yoke	Stator Teeth	Coil	End winding	Stator retaining sleeve	Rotor retaining sleeve	Permanent Magnet	Rotor yoke
1	INCONEL	76.77	83.94	90.95	88.44	91.77	69.85	69	67.78
2	Steel	102.3	113.5	119.7	116.1	124.9	93.44	92.28	90.54
3	Hastelloy	75.51	82.49	89.54	87.08	90.14	68.7	67.88	66.66
1	Titanium	68.69	74.61	81.87	79.69	81.28	61.43	61.6	60.56

Conclusion and Recommendations

Conclusion

- The eddy current loss in the stator retaining sleeve will be higher than the iron and copper loss when a metallic material is used. Hence a non-metallic material should be used in stator retaining sleeve.
- For rotor retaining sleeve, when the single sheet material is used the eddy current loss is less than 0.2% of the iron and copper loss, but when retaining sheet with two materials are used for example copper and Inconel the eddy current loss is 3.5%. Hence single sheet material should be used in the rotor retaining sleeve.
- As the loss in the rotor retaining sleeve is very small as compared to the iron and copper loss the temperature in the machine will remain almost the same for all type of materials used. Hence it is advisable to use steel as the retaining sleeve material because it is the cheapest material among the materials selected for analysis.
- The Joule loss in the stator-rotor gap due to MHD is just 0.00052% of the iron and copper loss for laminar flow under constant magnetic flux density, which is negligible, while the friction loss at the rotor surface is 0.1%. The MHD losses will be higher under the harmonic magnetic flux density, but the total MHD losses will not be substantial for low-speed machine due to the low electrical conductivity of the seawater.

Recommendations

- Eddy current losses calculation for fractional slot machine can be done to find a suitable sleeve material.
- The thermal model of the machine should be developed, in which axial flow of the heat in the water is considered. Also, the model for actual frame surface and endcap should be used so that better temperature understanding inside the machine.

- CFD analysis in the stator-rotor gap can be done to understand the fluid velocity under better turbulence condition.
- Seawater being electrically conductive can be used to generate electricity using MHD Principle. This could be one of the methods for ocean energy. But as the seawater conductivity is just $5S/m$, the MHD generator will not be economically attractive. But if we can increase the conductivity of the fluid then it will become interesting. [49] proposed the use of liquid metal as fluid. [50] proposed liquid metal MHD (LMMHD) wave energy direct conversion which has 67.5% conversion efficiency for wave amplitude of 1.0M. Further research needs to be done to make it more viable.

Appendix A

General solution of Laplace equation

The general solution of the Laplace equation by can be solve by considering the separation of the variable method as.

$$\frac{\partial^2}{\partial r^2}A(r, \theta) + \frac{1}{r} \frac{\partial}{\partial r}A(r, \theta) + \frac{1}{r^2} \frac{\partial^2}{\partial \theta^2}A(r, \theta) = 0 \quad (\text{A-1})$$

Attempt separation of variables by writing

$$A(r, \theta) = R(r)\Theta(\theta) \quad (\text{A-2})$$

$$\frac{d^2R}{dr^2}\Theta + \frac{1}{r} \frac{dR}{dr}\Theta + \frac{1}{r^2} \frac{d^2\Theta}{d\theta^2}R = 0 \quad (\text{A-3})$$

Multiplying both sides by $r^2/(R\Theta)$ we get

$$\left(\frac{r^2}{R} \frac{d^2R}{dr^2} + \frac{r}{R} \frac{dR}{dr} \right) \Theta + \left(\frac{1}{\Theta} \frac{d^2\Theta}{d\theta^2} \right) = 0 \quad (\text{A-4})$$

The solution of the Equation (A-4) must be periodic, so the differential equation is

$$\left(\frac{1}{\Theta} \frac{d^2\Theta}{d\theta^2} \right) = -n^2 \quad (\text{A-5})$$

which has solution

$$\Theta(\theta) = C_n \cos(n\theta) + D_n \sin(n\theta) \quad (\text{A-6})$$

Considering the equation again

$$\left(\frac{r^2}{R} \frac{d^2R}{dr^2} + \frac{r}{R} \frac{dR}{dr} \right) \Theta = n^2 \quad (\text{A-7})$$

The solution of the equation is

$$R(r) = A_n r^n + B_n r^{-n} \quad (\text{A-8})$$

for $n = 0$ the solution of radial equation is given as

$$R(r) = A_0 + B_0 \ln(r) \quad (\text{A-9})$$

Combining the solutions gives the general solution of Laplace equation.

$$A(r, \theta) = A_0 + B_0 \ln(r) + \sum_{n=1}^{\infty} [A_n r^n + B_n r^{-n}] [C_n \cos(n\theta) + D_n \sin(n\theta)] \quad (\text{A-10})$$

Appendix B

Star of slot method

Fractional slot winding machine gives several advantages, firstly fractional slot winding reduces manufacturing cost and end winding length. Secondly, it can be used when low speed is required as the machine can be designed with a high number of poles. Thirdly, it can be applied when low ripple torque is required, to reduce the periodicity between the number of slots and pole pairs.

Star of slot method is useful in designing the correct coil connections to maximize the main harmonics of the EMF induced in the winding of fractional slot synchronous machine with a large number of poles. Besides as the star of slots has information of the winding distribution, it can be adopted for analysis of the main harmonics, harmonic contents of the EMF waveform and harmonic content of air-gap MMF distribution.

The star of slots is the phasor representation of the main EMF harmonic induced on the coil side of each slot, characterized by Q/t spokes, with each spoke containing t phasors. The angle between the phasors of two adjacent slots is the electrical angle $\alpha_s^e = p\alpha_s$ where, α_s is the slot angle in mechanical radians, i.e. $\alpha_s = 2\pi/Q$. The angle between two spokes results in

$$\alpha_{ph} = \frac{2\pi}{(Q/t)} = \frac{\alpha_s^e}{p} t$$

Since electrical angles are considered, the star of slots refers to the equivalent two-pole machine. The number given to each phasor corresponds to the number given consecutively to each stator slot. The winding factor is calculated using the electromotive force phasors. The winding factor k_w for the fundamental can be calculated using the following [10].

$$K_W = \frac{|\sum_{i=1}^{2Q_s/3} \vec{E}_i|}{n_l Q_s/3} \quad (\text{B-1})$$

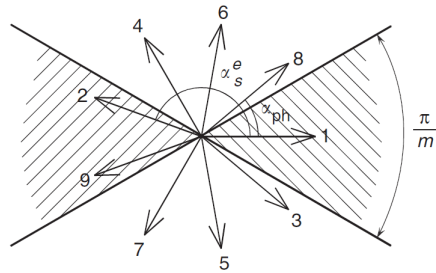


Figure B-1: Example of star of slots of machine with $Q = 9, 2p = 8$ [9]

Table B-1: Harmonic Orders(HO) of a single-layer winding [10]

Harmonic Order	Q/t even $Q/2t$ even	$Q/2t$ odd	Q/t odd
t even	$(2n - 1)t$	nt	$nt/2$
t odd	$(2n - 1)t$	nt	-

Appendix C

Magnetohydrodynamics

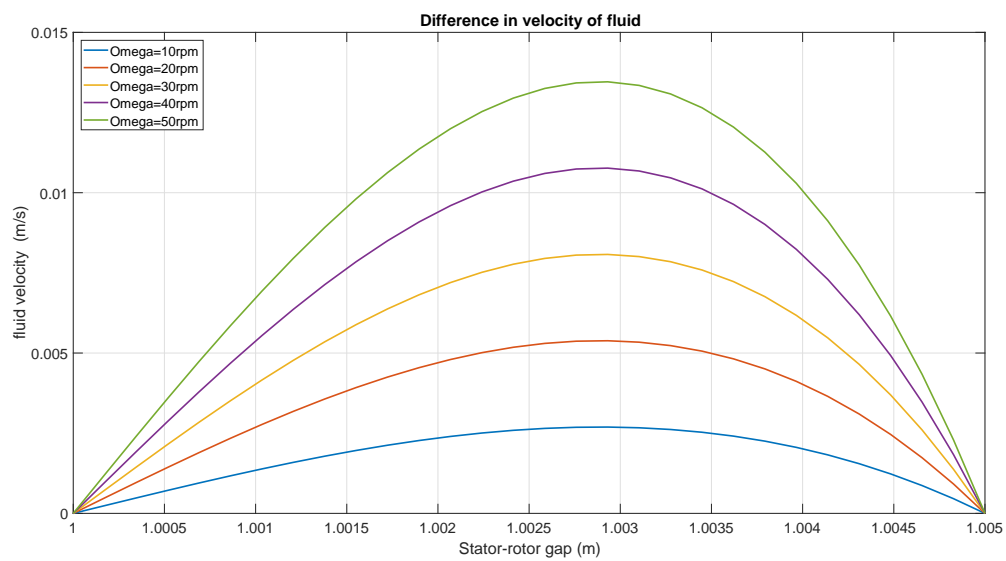


Figure C-1: Velocity variation seawater at different rotor velocity

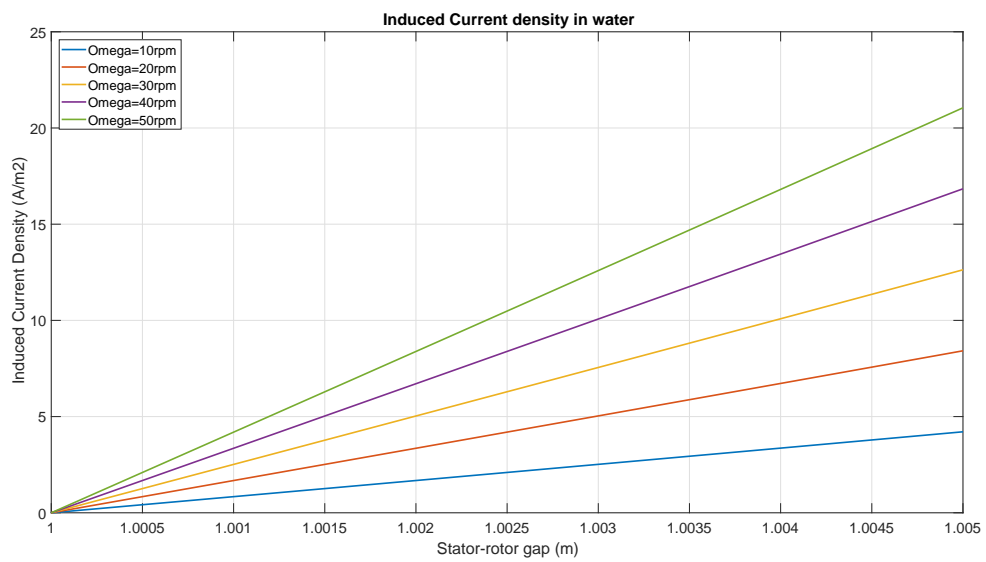


Figure C-2: Current Density in seawater at different rotor velocity

Appendix D

Thermal Model

Table D-1: Thermal resistances and their explanations of the network

Component	Explanation	Value
R_{th3}	Axial resistance from stator yoke to end cap air	0.7177
R_{th4}	Radial interconnecting resistance of the stator yoke	-5.8147e-05
R_{th5}	Radial resistance from stator yoke to frame	8.6956e-05
R_{th6}	Radial resistance from stator yoke to stator teeth	8.7487e-05
R_{th7}	Axial resistance from stator teeth to end cap air	0.3445
R_{th8}	Radial / circumferential resistance from stator teeth to stator winding	2.9778e-05
R_{th9}	Radial interconnecting resistance of the stator teeth	-5.1337e-04
R_{th10}	Radial resistance from stator teeth to stator yoke	7.5996e-04
R_{th11}	Radial resistance from stator teeth to stator air-gap	7.8076e-04
R_{th12}	Radial / circumferential resistance from the stator coils to stator teeth	0.0014
R_{th13}	Axial resistance from stator coils to end winding	6.7240e-04
R_{th14}	Radial resistance from stator coil to stator yoke	0.0029
R_{th15}	Radial resistance from stator coil to air-gap	0.0028
R_{th19}	Axial resistance from end winding to stator coil	1.5310e-04
R_{th20}	Resistance from end-winding to end-cap-air (legs)	0.0041
R_{th21}	Resistance from end-winding to end-cap-air (toroid)	-
R_{th22}	Axial resistance from end cap air to frame	2.8773e-04
R_{th23}	Axial resistance from end cap air to stator yoke	0.0021
R_{th24}	Resistance from end cap air to stator teeth	0.0011
R_{th25}	Resistance from end cap air to end winding	3.1910e-04
R_{th26}	Resistance from end cap air to rotor end rings	0.0040
R_{th27}	Resistance from end cap air to rotor iron	0.0026
R_{th29}	Axial Resistance from Permanent Magnet to end cap air	0.0537
R_{th30}	Radial interconnecting Resistance of Permanent Magnet	-7.1704e-05
R_{th31}	Radial Resistance from Permanent Magnet to rotor retaining sleeve	1.0735e-04

Continued on next page

Table D-1 – continued from previous page

Component	Explanation	Value
R_{th32}	Radial Resistance from Permanent Magnet to rotor yoke	1.0776e-04
R_{th50}	Radial Resistance of air between rotor retaining sleeve to rotor yoke	0.0502
R_{th33}	Axial Resistance from Rotor yoke to end cap air	0.8650
R_{th34}	Radial interconnecting Resistance of rotor yoke	-5.6768e-05
R_{th35}	Radial Resistance from Rotor yoke to permanent magnet	8.4900e-05
R_{th36}	Radial Resistance from Rotor yoke to shaft	8.5406e-05
R_{th37}	Radial Resistance from shaft to Rotor yoke	1.3224
R_{th38}	Axial Resistance from shaft to frame through bearings	2.6546
R_{th39}	Radial Resistance from rotor retaining sleeve to permanent magnet	3.2912e-05
R_{th40}	Radial Resistance from rotor retaining sleeve to air-gap	3.2886e-05
R_{th41}	Radial interconnecting Resistance of rotor retaining sleeve	-2.1933e-05
R_{th42}	Axial Resistance from rotor retaining sleeve to end cap air	0.3765
R_{th43}	Resistance from end cap air to rotor retaining sleeve	0.0193
R_{th44}	Radial Resistance of air-gap	0.0033
R_{th45}	Radial Resistance from stator retaining sleeve to air-gap	3.2707e-05
R_{th46}	Radial Resistance from stator retaining sleeve to stator teeth & coil	3.2682e-05
R_{th47}	Radial interconnecting Resistance of stator retaining sleeve	-2.1796e-05
R_{th48}	Axial Resistance from stator retaining sleeve to end cap air	0.3741
R_{th49}	Resistance from end cap air to stator retaining sleeve	0.0192
R_{th55}	Radial Resistance from rotor sleeve to air-gap	8.3405e-05
R_{th56}	Natural convection Resistance from stator to air gap	1.0832e-04
R_{th57}	Forced convection Resistance from stator to air gap	8.8365e-05
R_{th58}	Radiation Resistance from stator to air gap	0.7317
R_{rad}	Radiation Resistance from frame to ambient	0.1434
R_{th59}	Natural convection Resistance from frame to ambient	0.0049
R_{th60}	Forced convection Resistance from frame to ambient	0.0049

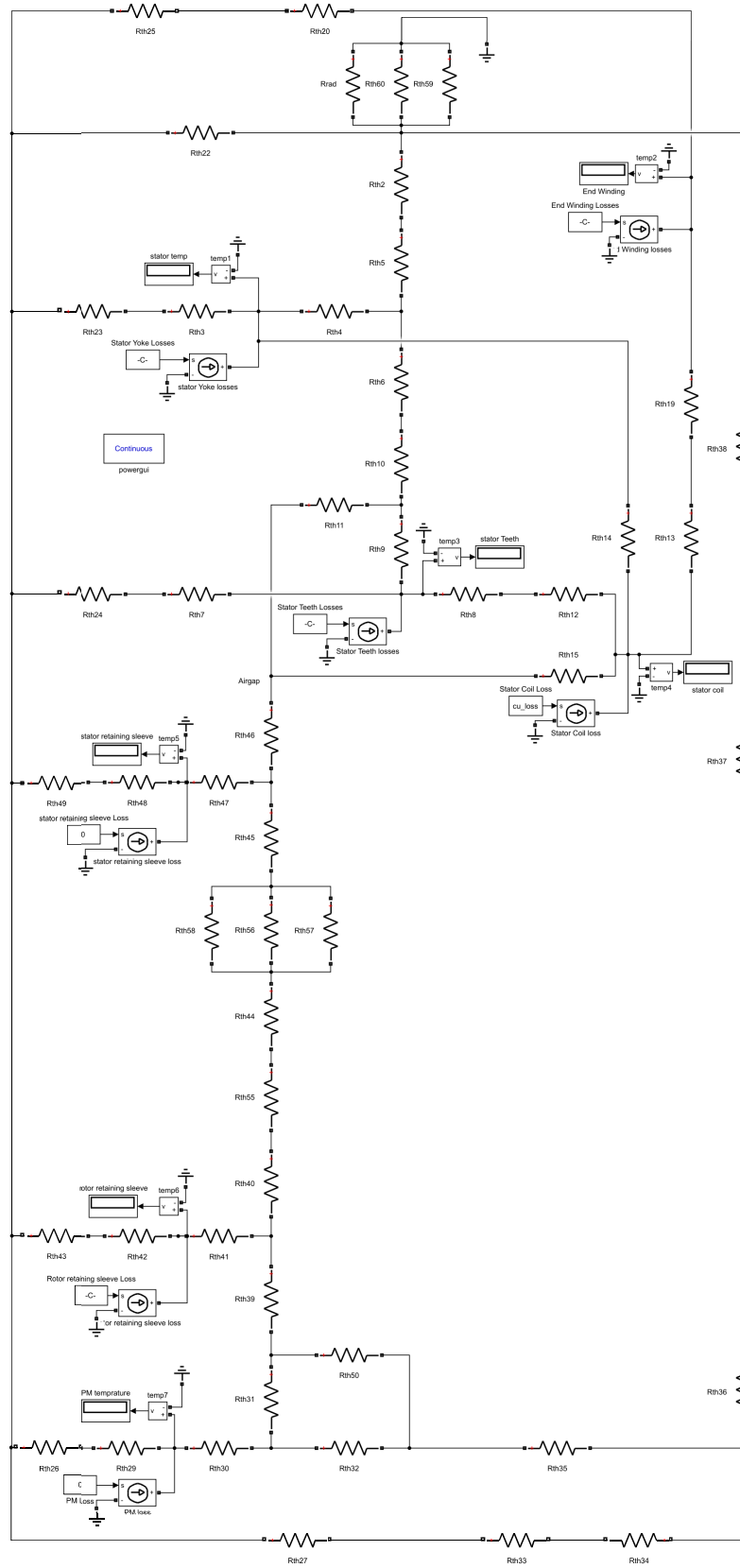


Figure D-1: Thermal Model of Machine

Bibliography

- [1] "Dutch marine energy," 2016. [Online]. Available: <http://dutchmarineenergy.com/>
- [2] F. Wani and H. Polinder, "A Review of Tidal Current Turbine Technology : Present and Future."
- [3] Z. Zhou, F. Scuiller, J. F. Charpentier, M. Benbouzid, and T. Tang, "An up-to-date review of large marine tidal current turbine technologies," *Proceedings - 2014 International Power Electronics and Application Conference and Exposition, IEEE PEAC 2014*, pp. 480–484, 2014.
- [4] L. Drouen, J. F. Charpentier, E. Semail, and S. Clenet, "A global approach for the design of a Rim-Driven marine turbine generator for sail boat," *2012 XXth International Conference on Electrical Machines*, pp. 547–553, 2012.
- [5] Z. Q. Z. Ackermann, D. Howe, E. Bolte, and B., "Instantaneous Magnetic Field Distribution in Brushless Permanent Magnet dc Motors, Part I: Open-circuit Field," *IEEE Transactions on Magnetics*, vol. 29, no. 1, pp. 124–135, 1993. [Online]. Available: <http://ieeexplore.ieee.org/lpdocs/epic03/wrapper.htm?arnumber=195560>
- [6] Z. Zhu and D. Howe, "Instantaneous magnetic field distribution in brushless permanent\nmagnet DC motors, Part III. Effect of stator slotting," *IEEE Transactions on Magnetics*, vol. 29, no. 1, pp. 143–151, 1993.
- [7] S. Poncet, S. Haddadi, and S. Viazzo, "Numerical modeling of fluid flow and heat transfer in a narrow Taylor-Couette-Poiseuille system," *International Journal of Heat and Fluid Flow*, vol. 32, no. 1, pp. 128–144, 2011.
- [8] P. Mellor, D. Roberts, and D. Turner, "Lumped parameter thermal model for electrical machines of TEFC design," *IEE Proceedings B Electric Power Applications*, vol. 138, no. 5, p. 205, 1991. [Online]. Available: <http://digital-library.theiet.org/content/journals/10.1049/ip-b.1991.0025>
- [9] N. Bianchi, S. Bolognani, M. D. Pre, and G. Grezzani, "Design considerations for fractional-slot winding configurations of synchronous machines," *IEEE Transactions on Industry Applications*, vol. 42, no. 4, pp. 997–1006, July 2006.

- [10] F. Libert and J. Soulard, "Investigation on pole-slot combinations for permanent-magnet machines with concentrated windings," *International Conference on Electrical Machines (ICEM 04)*, pp. 5–8, 2004. [Online]. Available: <http://www.ee.kth.se/php/modules/publications/reports/2004/IR-EE-EME{ }2004{ }005.pdf>
- [11] H. Chen, N. Ait-Ahmed, L. Moreau, M. Machmoum, and M. E. Zaim, "Performances analysis of a doubly salient permanent magnet generator for marine tidal current applications," in *Proceedings - 2014 International Power Electronics and Application Conference and Exposition, IEEE PEAC 2014*, 2014, pp. 320–325.
- [12] A. Uihlein and D. Magagna, "Wave and tidal current energy - A review of the current state of research beyond technology," *Renewable and Sustainable Energy Reviews*, vol. 58, pp. 1070–1081, 2016. [Online]. Available: <http://dx.doi.org/10.1016/j.rser.2015.12.284>
- [13] S. Djebbari, J. F. Charpentier, F. Scuiller, and M. Benbouzid, "Design and Performance Analysis of Double Stator Axial Flux PM Generator for Rim Driven Marine Current Turbines," *IEEE Journal of Oceanic Engineering*, vol. 41, no. 1, pp. 50–66, 2016.
- [14] O. K. Mueller, A. S. McDonald, and M., "A direct drive permanent magnet generator design for a tidal current turbine (SeaGen)," *2011 IEEE International Electric Machines Drives Conference (IEMDC)*, pp. 224–229, 2011. [Online]. Available: <http://ieeexplore.ieee.org/lpdocs/epic03/wrapper.htm?arnumber=5994850{ }5Cnhttp://ieeexplore.ieee.org/xpls/abs{ }all.jsp?arnumber=5994850>
- [15] T. M. Honshima, M. Yoshikawa, and M., "Improvement of the corrosion resistance on Nd-Fe-B magnet with nickel plating," *IEEE Transactions on Magnetics*, vol. 25, no. 5, pp. 3776–3778, 1989.
- [16] L. Schultz, A. M. El-Aziz, G. Barkleit, and K. Mummert, "Corrosion behaviour of Nd-Fe-B permanent magnetic alloys," *Materials Science and Engineering A*, vol. 267, no. 2, pp. 307–313, 1999. [Online]. Available: <http://www.scopus.com/inward/record.url?eid=2-s2.0-0032843186{ }&partnerID=tZOtx3y1>
- [17] D. J. B. Smith, B. C. Mecrow, G. J. Atkinson, A. G. Jack, and A. A. A. Mehna, "Shear stress concentrations in permanent magnet rotor sleeves," *The XIX International Conference on Electrical Machines - ICEM 2010*, pp. 1–6, 2010.
- [18] D. L. O. Lewis and A. W., "Generator requirements and functionality for ocean energy converters," *The XIX International Conference on Electrical Machines - ICEM 2010*, pp. 1–7, 2010.
- [19] T. J. Muhr, J. Fletcher, N. Hassanain, M. Mueller, and M., "Challenges to machine windings used in electrical generators in wave and tidal power plants," *2009 IEEE Conference on Electrical Insulation and Dielectric Phenomena*, pp. 238–241, 2009.
- [20] L. Drouen, J. F. Charpentier, E. Semail, and S. Clenet, "Study of an innovative electrical machine fitted to marine current turbines," *OCEANS 2007 - Europe*, pp. 1–6, 2007.
- [21] S. Djebbari, J. F. Charpentier, F. Scuiller, M. Benbouzid, and S. Guemard, "Rough design of a Double-Stator Axial Flux Permanent Magnet generator for a rim-driven marine current turbine," *IEEE International Symposium on Industrial Electronics*, pp. 1450–1455, 2012.

-
- [22] F. Z. F. Zhou, J. S. J. Shen, W. F. W. Fei, and R. L. R. Lin, "Study of Retaining Sleeve and Conductive Shield and Their Influence on Rotor Loss in High-Speed PM BLDC Motors," *IEEE Transactions on Magnetics*, vol. 42, no. 10, pp. 3398–3400, 2006.
- [23] W. Li, W. Jing, X. Zhang, and B. Kou, "Loss calculation and thermal analysis of three modes of retaining sleeves for high-speed PM generators," *Digests of the 2010 14th Biennial IEEE Conference on Electromagnetic Field Computation, CEFC 2010*, vol. 1, no. 10, p. 150040, 2010.
- [24] Y. Huang, J. Dong, L. Jin, J. Zhu, and Y. Guo, "Eddy-current loss prediction in the rotor magnets of a permanent magnet synchronous generator with modular winding feeding a rectifier load," *IEEE Transactions on Magnetics*, vol. 47, no. 10, pp. 4203–4206, 2011.
- [25] D. A. Atallah, Kais and Howe, David and Mellor, Philip H and Stone, "Rotor eddy-current loss in permanent-magnet brushless AC machines," *IEEE Transactions on Magnetics*, vol. 36, no. 9, pp. 1612–1618, 2000.
- [26] Y. Burkhardt, G. Huth, and S. Urschel, "Eddy current losses in PM canned motors," *The XIX International Conference on Electrical Machines - ICEM 2010*, pp. 1–7, 2010.
- [27] Y. p. L. Li, Y. I. Hu, X. Liu, and C. x., "Calculation and Analysis of Can Losses of Canned Induction Motor," *IEEE Transactions on Industrial Electronics*, vol. 61, no. 9, pp. 4531–4538, 2014.
- [28] Q. Yu, X. Wang, and Y. Cheng, "Electromagnetic Calculation and Characteristic Analysis of Can Effect of a Canned Permanent Magnet Motor," *IEEE Transactions on Magnetics*, vol. 52, no. 12, 2016.
- [29] M. R. Shah and A. M. EL-Refaie, "Eddy-current loss minimization in conducting sleeves of surface PM machine rotors with fractional-slot concentrated armature windings by optimal axial segmentation and copper cladding," *IEEE Transactions on Industry Applications*, vol. 45, no. 2, pp. 720–728, 2009.
- [30] M. R. J. Nerg and J. Pyrhonen, "Thermal Analysis of Radial-Flux Electrical Machines With a High Power Density," *IEEE Transactions on Industrial Electronics*, vol. 55, no. 10, pp. 3543–3554, 2008. [Online]. Available: <http://ieeexplore.ieee.org/stamp/stamp.jsp?tp=&arnumber=4555649&isnumber=4636792>
- [31] H. Rouhani, J. Faiz, and C. Lucas, "Lumped thermal model for switched reluctance motor applied to mechanical design optimization," *Mathematical and Computer Modelling*, vol. 45, no. 5-6, pp. 625–638, 2007.
- [32] A. B. Nachouane, A. Abdelli, G. Friedrich, and S. Vivier, "Numerical study of convective heat transfer in the end regions of a totally enclosed permanent magnet synchronous machine," *IEEE Transactions on Industry Applications*, vol. 53, no. 4, pp. 3538–3547, July 2017.
- [33] H. Menana, J. F. Charpentier, and C. Gabillet, "Contribution to the mhd modeling in low speed radial flux ac machines with air-gaps filled with conductive fluids," *IEEE Transactions on Magnetics*, vol. 50, no. 1, pp. 1–4, Jan 2014.
- [34] A. Grauers, "Design of Direct-driven Permanent-magnet Generators for Wind Turbines," Ph.D. dissertation, Chalmers University of Technology, 1996. [Online]. Available: <http://webfiles.portal.chalmers.se/et/PhD/GrauersAndersPhD.pdf>

- [35] V. Pyrhonen, Juha and Jokinen, Tapani and Hrabovcova, *Design of rotating electrical machines*, 1st ed. John Wiley & Sons, 2008.
- [36] V. Leivsdottir, “Investigation of Loss Calculation Methods for PMSMs and Implementation of Loss Functionality on a Developed FEM Model,” Ph.D. dissertation, Norwegian University of Science and Technology, 2016.
- [37] H. Vu Xuan, D. Lahaye, H. Polinder, and J. A. Ferreira, “Influence of stator slotting on the performance of permanent-magnet machines with concentrated windings,” *IEEE Transactions on Magnetics*, vol. 49, no. 2, pp. 929–938, 2013.
- [38] Z. Q. Zhu and D. Howe, “Instantaneous magnetic field distribution in permanent magnet brushless DC motors. IV. Magnetic field on load,” *IEEE Transactions on Magnetics*, vol. 29, no. 1, pp. 152–158, 1993.
- [39] J. M. Yon, P. H. Mellor, R. Wrobel, J. D. Booker, and S. G. Burrow, “Analysis of semipermeable containment sleeve technology for high-speed permanent magnet machines,” *IEEE Transactions on Energy Conversion*, vol. 27, no. 3, pp. 646–653, 2012.
- [40] E. Gellert and D. Turley, “Seawater immersion ageing of glass-fibre reinforced polymer laminates for marine applications,” *Composites Part A: Applied Science and Manufacturing*, vol. 30, no. 11, pp. 1259–1265, 1999.
- [41] Z. Q. Zhu, K. Ng, N. Schofield, and D. Howe, “Analytical prediction of rotor eddy current loss in brushless machines equipped with surface-mounted permanent magnets. I. Magnetostatic field model,” *ICEMS 2001 - Proceedings of the 5th International Conference on Electrical Machines and Systems*, vol. 2, no. 1, pp. 806–809, 2001.
- [42] J. J. S. Shang, *Computational Electromagnetic-Aerodynamics*. Wiley-IEEE Press, 2016. [Online]. Available: <http://ieeexplore.ieee.org/xpl/articleDetails.jsp?arnumber=7471036>
- [43] A. Boglietti, A. Cavagnino, M. Lazzari, and M. Pastorelli, “A Simplified Thermal Model for Variable-Speed Self-Cooled Industrial Induction Motor,” *IEEE Transactions on Industry Applications*, vol. 39, no. 4, pp. 945–952, 2003.
- [44] A. B. Nachouane, A. Abdelli, G. Friedrich, and S. Vivier, “Estimation of windage losses inside very narrow air gaps of high speed electrical machines without an internal ventilation using cfd methods,” pp. 2704–2710, Sept 2016.
- [45] Z. J. Liu, D. Howe, P. H. Mellor, and M. K. Jenkins, “Thermal analysis of permanent magnet machines,” *Electrical Machines and Drives, 1993. Sixth International Conference on (Conf. Publ. No. 376)*, pp. 359–364, 1993.
- [46] D. P. Incropera, Frank P and Dewitt, *Introduction to Heat Transfer*, F. Edition, Ed. John WHey & Sons. New York. NY, 1996.
- [47] J. Puranen, “Induction Motor Versus Permanent Magnet Synchronous Motor in Motion Control Applications : A Comparative Study,” Ph.D. dissertation, Lappeenranta University of Technology, 2006. [Online]. Available: <https://www.doria.fi/bitstream/handle/10024/31238/tmp.objres.448.pdf?sequence=1>

- [48] H. Vu Xuan, "Modeling of exterior rotor permanent magnet machines with concentrated windings," Ph.D. dissertation, Delft University of Technology, 2012. [Online]. Available: <https://repository.tudelft.nl/islandora/object/uuid{%}3A27bb59c4-14c8-45fe-9284-28363b46e060>
- [49] W. D. Jackson, "Liquid-metal faraday-type MHD generators," *Power Apparatus and Systems, IEEE Transactions on*, vol. 82, no. 69, pp. 904–907, 1963.
- [50] Z. L. Y. P. L. Z. C. S. R. L. Y. X. B. L. Jian Li and J. Jia, "Analysis of liquid metal MHD wave energy direct conversion system," *The Eighteenth International Offshore and Polar Engineering Conference*, vol. 8, pp. 388–392, 2008.

